



UNIVERSIDAD DE INVESTIGACIÓN DE TECNOLOGÍA EXPERIMENTAL YACHAY

Escuela de Ciencias Biológicas e Ingeniería

TÍTULO: Synthesis and Characterization of Alginate/Gelatin Bioinks for 3D Human Tissue Models

Trabajo de integración curricular presentado como requisito para la
obtención del título de Ingeniero Biomédico

Autor:

Alicia del Rocío Bonilla Vázquez

Tutor:

PhD. Sarah Briceño

Co-tutor:

PhD. Elsa Materón

Urcuquí, diciembre 2023

Autoría

Yo, **Alicia del Rocío Bonilla Vázquez**, con cédula de identidad 0302199864, declaro que las ideas, juicios, valoraciones, interpretaciones, consultas bibliográficas, definiciones y conceptualizaciones expuestas en el presente trabajo; así cómo, los procedimientos y herramientas utilizadas en la investigación, son de absoluta responsabilidad de la autora del trabajo de integración curricular. Así mismo, me acojo a los reglamentos internos de la Universidad de Investigación de Tecnología Experimental Yachay.

Urcuquí, diciembre 2023.

Alicia del Rocío Bonilla Vázquez
CI:0302199864

Autorización de publicación

Yo, **Alicia del Rocío Bonilla Vázquez**, con cédula de identidad 0302199864, cedo a la Universidad de Investigación de Tecnología Experimental Yachay, los derechos de publicación de la presente obra, sin que deba haber un reconocimiento económico por este concepto. Declaro además que el texto del presente trabajo de titulación no podrá ser cedido a ninguna empresa editorial para su publicación u otros fines, sin contar previamente con la autorización escrita de la Universidad.

Asimismo, autorizo a la Universidad que realice la digitalización y publicación de este trabajo de integración curricular en el repositorio virtual, de conformidad a lo dispuesto en el Art. 144 de la Ley Orgánica de Educación

Urcuquí, diciembre 2023.

Alicia del Rocío Bonilla Vázquez
CI:0302199864

Acknowledgements

Life is full of challenges, and every decision we make marks a before and after in the person we long to be. Without a doubt, we are not alone on the path of life. There are many people who encourage us, opportunities that make us grow, and lessons we learn daily.

First, I would like to thank God and the Virgin of the Cloud for blessing and illuminating my path. To my parents, Fanny and Luis, who have been my example of perseverance and the fundamental pillar to carry out my goals and objectives. Thanks to your unconditional support since I decided to study at Yachay. To my brother, Giancarlo, who made me smile in the dark moments. Despite the distance, I never felt alone because my family encouraged me to move forward with every word of encouragement and gesture of affection. I want to thank my thesis tutor, Sarah Briceño, PhD., who has supported me in all the unforeseen events and changes during this last stage. Thank you to each of my teachers throughout my career for being such excellent professionals and human beings.

My sincere thanks to the University of São Paulo, Institute of Physics and Institute of Chemistry of São Carlos for the opportunity to be part of their research projects, and thanks for providing me with the help and the resources used in this work. A special thanks to Elsa Materón, PhD., my mentor at the São Carlos Physics Institute; she has inspired me to continue in the research world. During my stay, she was the one who taught me the most about the nano world and got involved in her projects that are truly fascinating and contribute to science. I also thank Amanda Maciel, who taught me and helped me in the studies carried out in this work.

At the university, we found a second family who are friends. They accompanied us in the classrooms and brightened our life on campus. Thank Mishi for giving me her unconditional support. More than just a friend, I consider her my sister because she has been there through thick and thin, through my cries of joy and sadness. Living on campus would not have been the same without my dear roommate. Vero (Messi) will always have a special place in my heart, a friend I greatly appreciate; thank you for the home remedies for my illnesses. The Divinas of H-33 will always be in my heart. I love them very much. I also want to thank the "Las Populares" team, Dani, Les and Sam, my career friends with whom I have shared many experiences inside and outside the classroom. The "Frink" team, Saul, Franklin and Mishi, are unique people I greatly appreciate. What united Lobos in Physics I was not separated by the different careers we decided to study. Let's go, team!

Brazil allowed me to learn and experience the world of science and research much more closely, but I also met exceptional people. One of them was Aaron, my motivational coach and friend, who has given me his moral support; we are a WhatsApp away. Thank you.

Thank you also to all the people who have contributed and added to my life. Thank you for believing in me when I didn't even do it. I will carry you in my heart and wish success to each of you.

Alicia Bonilla Vázquez

Resumen

Actualmente, la probabilidad de que un fármaco en tratamientos contra el cáncer pase los ensayos clínicos es baja porque se prueban en modelos animales o cultivos celulares 2D, que no proporcionan un sistema preciso. Los investigadores han visto los modelos de tejidos 3D como una alternativa para la investigación oncológica ya que, con la bioimpresión 3D, se pueden generar estos modelos que ayudan a recrear entornos tumorales, permitiendo estudiar el comportamiento de los fármacos. Por tanto, el objetivo es sintetizar biotintas con características como biocompatibilidad, biodegradabilidad, no toxicidad, no inmunogenicidad e integridad mecánica. El presente trabajo estudia la viabilidad, morfología y composición de hidrogeles basados en alginato y gelatina entrecruzados con CaCl₂ y genipina. Los hidrogeles se sintetizaron a partir de polímeros naturales como el alginato de sodio y la gelatina utilizando métodos de reticulación iónicos y naturales. Las muestras se caracterizaron mediante ensayos ATR-FTIR, SEM y MTT para determinar la viabilidad celular. Los resultados obtenidos revelaron que las líneas celulares Caco-2 y HUVEC con las que se puede desarrollar un modelo de tejido para evaluar fármacos contra el cáncer colorrectal mostraron una mejora de los resultados en los hidrogeles de gelatina, alginato y CaCl₂ (68,92%) y en la gelatina, alginato, hidrogeles con genipina al 0,25% p/v (60% en HUVEC y 75,07% en Caco-2). Los resultados obtenidos demuestran el uso potencial de biotintas de alginato/gelatina para modelos 3D de tejido humano.

Palabras clave: Biotintas, hidrogeles, modelos de tejidos 3D, bioimpresión 3D, genipina.

Abstract

Currently, the likelihood of a drug in cancer treatments passing clinical trials is low because they are tested in animal models or 2D cell cultures, which do not provide a precise system. Researchers have seen 3D tissue models as an alternative for oncological research since, with 3D bioprinting, these models can be generated that help recreate tumor environments, allowing the behavior of drugs to be studied. Therefore, the aim is to synthesize bioinks with characteristics such as biocompatibility, biodegradability, non-toxicity, non-immunogenicity, and mechanical integrity. The present work studies hydrogels' viability, morphology, and composition based on alginate and gelatin crosslinked with $CaCl_2$ and genipin. The hydrogels were synthesized based on natural polymers such as sodium alginate and gelatin using ionic and natural crosslinking methods. The samples were characterized using ATR-FTIR, SEM, and MTT assay for cell viability. The obtained results revealed that the Caco-2 and HUVEC cell lines with which a tissue model can be developed to evaluate colorectal cancer drugs showed an improvement of the results in the gelatin, alginate, and $CaCl_2$ hydrogels (68.92%) and the gelatin, alginate hydrogels with genipin at 0.25% w/v (60% in HUVEC and 75.07% in Caco-2). The results obtained demonstrate the potential use of alginate/gelatin bioinks for 3D human tissue models.

Keywords: Bioink, hydrogels, 3D tissue models, 3D bioprinting, genipin.

Contents

List of Figures	viii
List of Tables	x
1 Introduction	1
2 Motivation	5
2.1 Problem Statement	5
2.2 General and Specific Objectives	6
2.2.1 General Objective	6
2.2.2 Specific Objectives	6
3 Theoretical Background	7
3.1 3D Human tissue models	7
3.2 3D Bioprinting for tissue engineering	8
3.2.1 Extrusion 3D bioprinting	8
3.2.2 Inkjet 3D bioprinting	9
3.2.3 Laser-assisted bioprinting	9
3.3 Bioink	9
3.3.1 Hidrogel-based bioink	10
3.3.2 Crosslinking of hydrogels	10
3.3.3 Requirements for bioink formulation	12
3.3.4 Sodium alginate	13
3.3.5 Gelatin	14
3.4 Composites	15
3.4.1 Alginate/gelatin composite	15
3.5 Genipin crosslinking mechanism	16
3.6 Techniques of characterization and optimization of biomaterials	18
3.6.1 Fourier Transform Infrared spectroscopy (FT-IR)	18

3.6.2	Scanning electron microscope (SEM)	19
3.6.3	Biological characterization	21
3.7	Cell lines	22
3.7.1	Caco-2	22
3.7.2	HUVEC	23
4	Methodology	25
4.1	Synthesis of bioinks	25
4.1.1	Hydrogel preparation	25
4.2	Characterization	28
4.2.1	FT-IR spectroscopy	28
4.2.2	SEM	28
4.3	Cell culture	29
4.3.1	Culture conditions for Caco-2	29
4.3.2	Culture conditions for HUVEC	29
4.4	Cell viability	30
4.4.1	Trypan blue exclusion assay	30
4.4.2	MTT assay for hydrogels	31
5	Results & Discussion	35
5.1	FT-IR spectroscopy	35
5.2	Morphology of hydrogels	40
5.3	Cell viability of alginate and gelatin hydrogels	44
5.4	Optical microscopy of cells lines	48
5.4.1	HUVEC cells	48
5.4.2	Caco-2 cells	54
6	Conclusions & Outlook	61
	Bibliography	63

List of Figures

3.1	Bioprinting techniques	8
3.2	Chemical structure of sodium alginate	14
3.3	Chemical structure of gelatin	15
3.4	Chemical structure of genipin	16
3.5	Crosslinking mechanism of Genipin	18
3.6	Principles of the Fourier-Transform Infrared Spectroscopy (FT-IR)	19
3.7	Diagram of components of SEM microscope.	20
3.8	Trypan blue assay	21
3.9	Reduction of MTT to formazan	22
3.10	Morphology of Caco-2 cell line	23
3.11	Morphology of HUVEC cell line	23
4.1	Set up of hydrogel preparation	25
4.2	Sodium alginate crosslinking with genipin	26
4.3	Hydrogels composites crosslinking with genipin	26
4.4	FT-IR Spectrometer Bruker Optik GmbH Tensor 27	28
4.5	Benchtop freeze dryer LS 3000 Terroni	28
4.6	LEO 440 Scanning Electron Microscope	29
4.7	Caco-2 cells with trypan blue	30
4.8	Cells cultivated in hydrogels	31
4.9	Thermo Scientific™ Varioskan™ LUX multimode microplate reader	32
4.10	Olympus CKX41 Inverted Microscope	32
5.1	FT-IR spectra of sodium alginate	35
5.2	FT-IR spectra of gelatin	36
5.3	FT-IR spectra of gelatin and sodium alginate solved in DPBS	37
5.4	FT-IR spectra of gelatin and sodium alginate with $CaCl_2$	38
5.5	FT-IR spectra of sodium alginate with genipin	39
5.6	FT-IR spectra of sodium alginate and gelatin with genipin	40

5.7	SEM microphotographs of hydrogel	41
5.8	SEM microphotographs of hydrogel	41
5.9	SEM microphotographs of hydrogel	42
5.10	SEM microphotographs of hydrogel	42
5.11	SEM microphotographs of hydrogel	43
5.12	SEM microphotographs of hydrogel	43
5.13	Cell viability of HUVEC and Caco-2 cells	44
5.14	Cell viability of HUVEC and Caco-2 cells	45
5.15	Cell viability of HUVEC and Caco-2 cells	46
5.16	Cell viability of HUVEC and Caco-2 cells	47
5.17	Optical microscopy of HUVEC cells	48
5.18	Optical microscopy of HUVEC cells	49
5.19	Optical microscopy of HUVEC cells	50
5.20	Optical microscopy of HUVEC cells	51
5.21	Optical microscopy of HUVEC cells	52
5.22	Optical microscopy of HUVEC cells	53
5.23	Optical microscopy of Caco-2 cells	54
5.24	Optical microscopy of Caco-2 cells	55
5.25	Optical microscopy of Caco-2 cells	56
5.26	Optical microscopy of Caco-2 cells	57
5.27	Optical microscopy of Caco-2 cells	58
5.28	Optical microscopy of Caco-2 cells	58

List of Tables

3.1 Advantages and disadvantages of materials used for 3D bioprinting.	11
4.1 Compositions of hydrogels.	27

Chapter 1

Introduction

Three-dimensional (3D) tissue printing, or bioprinting, has emerged as a revolutionary tool in tissue engineering and regenerative medicine. This technology has encouraged the production of 3D human tissue models, transforming how research is approached in this field. However, the success of bioprinting lies in the quality of the bioinks, especially the hydrogels, which serve as the vital environment for diverse cell populations during the biomanufacturing process¹.

Developing 3D tissue models aims to study and thoroughly understand drug behavior and complex dynamic interactions between cell-cell and cell-matrix. It is already possible thanks to bioprinting that helps to recreate tumor environments, and that is why oncological research and personalized medicine seek to develop these more precise models that would be used as preclinical, experimental systems in order to replace conventional two-dimensional (2D) animal models and cell cultures since the rates of translation of new drugs to the clinic are disappointingly low.

In oncology, a new drug's probability of successfully passing all clinical trial phases is 3.4%². If there is taking into account the failure of the current *in vivo* and *in vitro* models, then the probability is reduced to 0.1%³. These failures result in inefficient treatment, unsatisfactory patient cure rates, and economic losses incurred in each study. As a solution to this problem, 3D tissue models similar to the *in vivo* tumor have been proposed to achieve higher predictive rates of the response of a drug in preclinical processes, especially cancer, as proposed by Sbirkov and his team by developing a 3D bioprinting design of colorectal cancer⁴. The scientific community is intrigued by this model because limited bioprinted models are available for this particular type of cancer. It accounts for approximately 10% of all recently diagnosed malignancies, ranking as the third most prevalent cancer in both genders, following lung and breast cancer⁵.

Recent research in bioprinting for producing these models has posed challenges in formulating optimal bioinks for the bioprinting process⁶. Bioinks must possess several fundamental characteristics, including biocompatibility, biodegradability, non-toxicity, non-immunogenicity, printability, and mechanical integrity⁷. Although considerable focus has been placed on optimizing the physical properties of the ink, the study of the biological properties of biomaterials, whose function is to provide support and protection to cells both during and after the process, has been largely relegated to fabric construction¹. The mechanical and rheological properties of bioinks currently generate tissue structures with adequate mechanical strength, high shape fidelity, and notable robustness. However, it is

important to highlight that greater ease of printing bioinks is usually associated with lower cell viability during the bioprinting process, ultimately limiting their applications⁸.

According to the literature, the biomaterials used to make inks are polymers from natural sources because they imitate a native microenvironment and are favorable in cell adhesion, proliferation, migration and differentiation processes. Among the most used are collagen, alginate, gelatin and hyaluronic acid, which can be combined to compensate for the properties that the other polymer does not possess⁷. It is the case of the combination of gelatin with alginate. The reason why alginate is combined with other biomaterials is because it lacks characteristics such as biodegradability and adherence. While gelatin is cell-friendly as it has Arg-Gly-Asp (RGD) motifs that aid cell migration and attachment, it has low mechanical properties provided by alginate when they are combined⁷. In addition, they are low cost and have advantages such as non-antigenicity, biodegradability, bioactivity (RGD), gelation at low temperatures, thermo-reversibility, ease of processing, and non-toxicity, reasons why these combined materials have been used in various models⁹. For example, Zhao et al. used alginate and gelatin hydrogels with human gastric epithelial cells and smooth muscle cells in tissue models for gastric wound repair¹⁰. Chaji et al. proposed several alginate combinations where they studied their rheological characteristics and loaded breast cancer cells and adipocytes, managing to imitate the tissue rigidity observed in a physiological environment of breast cancer tumors¹¹. On the other hand, Hiller et al. optimized the bioink compounds to print human liver cells with an extrusion printer, generating a liver model for infection with human adenovirus 5 and transduction studies by an adeno-associated virus vector¹². For the 3D printing of angular scaffolds for cardiac tissue, Ketabat et al. optimized the characteristics of the printability properties of gelatin and alginate compounds with endothelial and cardiac cells, as well as their biological properties, in order to create a native heart¹³. Mondal et al. developed a sodium alginate-gelatin hydrogel by optimizing rheological parameters to print co-cultures of xenograft cells derived from non-small cell lung cancer (NSCLC) patients and lung cancer-associated fibroblasts¹⁴. It can be used to study high-throughput drug screening and other preclinical applications. These studies have optimized the rheological parameters by establishing the proportions and concentrations of hydrogels to load the cells and print the desired tissue, and considering that the rheological parameters in alginate concentrations between 2 and 4% and in gelatin between 4 and 6% provide good printability properties. The present study synthesizes alginate and gelatin hydrogels with these concentrations in different solvents, such as distilled water and Dulbecco's Phosphate Buffered Saline (DPBS) using ionic crosslinking methods with $CaCl_2$ and natural crosslinking with genipin. It is important to mention that these two types of solvents are used because the solvents used to prepare hydrogels also determine their mechanical properties and influence cell viability¹⁵. The biomaterials were characterized using attenuated total reflectance-Fourier transform infrared (ATR-FTIR) spectroscopy to evaluate these inks' behavior and study their chemical properties. In addition, cell viability was studied through an MTT (3-(4, 5-dimethylthiazolyl-2)-2, 5-diphenyltetrazolium bromide) assay in cell lines such as Caco-2 (Cancer coli-2) and human umbilical vein endothelial cells (HUVEC), which would be used to implement a tumor model of colorectal cancer and other digestive tumors. Finally, the morphological characteristics of the prepared hydrogels were analyzed with scanning electron microscopy (SEM).

This work studies hydrogels' viability, morphology, and composition based on alginate and gelatin crosslinked with $CaCl_2$ and genipin as potential bioinks for 3D human tissue models. Our results revealed that the Caco-2 and HUVEC cell lines, with which a tissue model can be developed to evaluate drugs against colorectal cancer,

have greater viability in hydrogels composed of gelatin, alginate and $CaCl_2$ (68.92% viability in HUVEC) and in the gelatin and alginate hydrogels with genipin 0.25% v/v (60% and 75.07% viability in HUVEC and Caco-2, respectively).

Chapter 2

Motivation

2.1 Problem Statement

Currently, the probability that a new drug for cancer treatment will pass the different phases of clinical trials is very low because conventional animal models and 2D cell cultures do not provide a precise experimental system, and translating new drugs to the clinic becomes challenging. Therefore, the scientific community seeks to develop 3D tissue models through the bioprinting technique since it helps to recreate tumor environments useful for oncological research and personalized medicine, allowing the study of the behavior of drugs and the complex dynamic interactions between cells and between cells and matrices providing more accurate models for clinical trials.

However, the greatest challenge in generating tissue models through 3D bioprinting is synthesizing optimal bioinks with characteristics such as biocompatibility, biodegradability, non-toxicity, non-immunogenicity, printability and mechanical integrity. In the development of bioinks, these characteristics have generated controversies because the relationship between the mechanical properties of the bioink and cell viability during bioprinting causes limitations. In some bioinks, the mechanical and rheological properties can generate tissue constructions with adequate mechanical resistance, high shape fidelity and robustness, providing better bioink printability. However, this can cause lower cell viability during bioprinting. For this reason, researchers still seek to optimize the trade-off of appropriate concentrations and proportions to achieve the reliability of the inks on both edges.

2.2 General and Specific Objectives

2.2.1 General Objective

This research aimed to obtain hydrogels based on natural polymers such as sodium alginate and gelatin using ionic and natural crosslinking methods and characterize them to analyze their properties to develop a 3D tissue model with Caco-2 and HUVEC cell lines.

2.2.2 Specific Objectives

- Synthesize hydrogels based on sodium alginate and gelatin.
- Evaluate different concentrations of genipin as natural cross-linking.
- Characterize the samples using Fourier Transform Infrared spectroscopy (FT-IR) and Scanning electron microscopy (SEM).
- Evaluate the viability of Caco-2 and HUVEC cells in hydrogels using MTT assay.

Chapter 3

Theoretical Background

3.1 3D Human tissue models

Over the years, to treat human diseases and disorders, researchers have used methods such as experimental animal, tissue and cell cultures, complementing them with computational simulations and clinical studies¹⁶. However, some of these methods have disadvantages; in the case of animal models, the difference in the biokinetic parameters, such as the absorption or distribution of the chemicals/substances, how the substances are metabolized, or the extrapolation of the results to humans due to the short life span of the animals so that the development of diseases cannot be precisely controlled¹⁷. In vitro procedures have been carried out for pharmacological, toxicological and medical science studies¹⁸.

Especially in toxicological testing, there has been a shift from animal models to 2D human cell cultures, which also have limitations by not providing cell-cell and cell-matrix interactions¹⁷. Therefore, with the latest advances, the adaptation of 3D in vitro human test models is developed. These in vitro 3D tissue models would function as complex systems that can improve the reliability and accuracy of test results. So, factors such as large-scale cell manufacturing and advanced manufacturing platforms must be considered¹⁹, as challenges such as widespread use and optimal reproduction of the models are faced.

There are several techniques for manufacturing and characterizing 3D tissue models, which can offer the ability to study complex mechanisms of disease progression and be a platform for drug testing. Within 3D tissue models, there are two types: those based on scaffolds such as spheroids, organoids and cell sheets, and on the other hand, we have anchorage-dependent models based on scaffolds²⁰. The technologies used to generate scaffolds are solvent-cast particle leaching (SCPL), electrospinning, and 3D bioprinting²⁰. In addition to the techniques, it is necessary to consider other parameters, such as the biomaterials to be used, which must be characterized and optimized for the formation of the native tissue. Incorporating cells that can be seeded or encapsulated within a biomaterial is essential to functionalize the tissue or organ of interest.

3.2 3D Bioprinting for tissue engineering

3D bioprinting is a process to create biomedical structures using living cells, biological chemicals, and biomaterials²¹. Currently, this is a technique that contributes to tissue engineering and regeneration. It could open up a new window in personalized medicine by printing organs with patients' cells and reducing the need for organ donations⁷.

3D printing allows load cells in materials layer by layer to create complex tissue constructs mimicking native tissue¹³. 3D bioprinting uses a bioink where cells can live, proliferate and generate specific tissue and organ.⁷ Three variables were used for the bioimpression of alive and functional tissue constructs. These are a cellular component, the supporting biomaterials as proteins and polymers, and the bioprinting corresponding to the manufacturing process⁷. 3D bioprinting provides flexibility to adjust key aspects such as bioink composition, printing speed, nozzle diameter, extrusion pressure and scaffold structure. Although a wide variety of biomaterials are available for this technique, each one has particular characteristics that require optimization to produce adequate structures.

The biomaterial's geometry will take in 3D bioprinting, which is designed using computer-aided design software or by geometries extracted from medical images²⁰. There are several bioprinting techniques through which cell-laden biomaterials called bioinks are delivered. These include extrusion, inkjet, and laser-assisted bioprinting²² as shown in Figure 3.1.

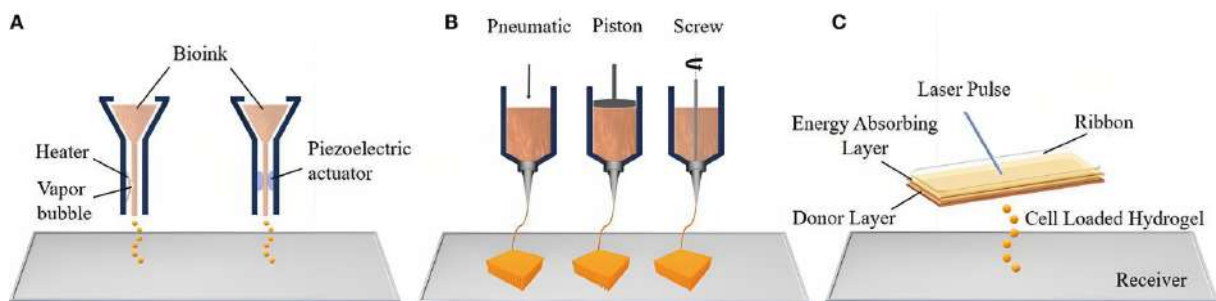


Figure 3.1: Bioprinting techniques: A) inkjet bioprinting, B) extrusion bioprinting, and C) laser-assisted bioprinting. Adapted from Tamay et al.²³

3.2.1 Extrusion 3D bioprinting

Extrusion bioprinting operates by dispensing bioink through either pneumatic (air pressure) or mechanical (screw or piston) systems²³. In the pneumatic approach, the bioink is pushed out of the nozzle or needle in a continuous cylindrical form by applying a constant air pressure. This results in a product with robust structural integrity. On the other hand, the mechanical system allows for more precise control over the bioink flow, thanks to the screw mechanism responsible for extrusion. This method enables the printing of tissues using various types of bioinks, including hydrogels carrying cells, microcarriers, and cell clusters²⁴. However, it is worth noting that cells may experience elevated mechanical stresses during the extrusion process, potentially reducing their viability.

Additionally, common challenges in bioprinting involve nozzle blockage due to cell clumping, high viscosity of the ink, or drying of the injected material within the nozzle²³.

3.2.2 Inkjet 3D bioprinting

Inkjet bioprinting allows a specific amount of colloidal solutions or cell suspensions to be placed at a high shear rate as droplets on a substrate to form a layer. Depending on the mode in which the ink is ejected, the printers are classified into continuous mode and drop-on-demand (DOD) mode²⁵. Depending on the actuator, this bioprinting model is divided into thermal and piezoelectric. In thermal inkjet printing, the temperature of the bioink is changed to generate pressure inside the print cartridge, forcing the bioink to pass through the output opening of the print head. In contrast, a piezoelectric inkjet printer with an acoustic wave or a physical component that changes shape or size causes pressure variations within the cartridge.

3.2.3 Laser-assisted bioprinting

Laser-based bioprinting uses the energy of a laser beam emitted from a source that heats the biomaterials printed on a metal film²⁶. The film's biological materials in liquid form are evaporated by laser energy and deposited on the substrate as droplets²⁷. This substrate may consist of a biopolymer or a culture medium that promotes the adhesion and growth of the deposited cells. The typical wavelength of lasers falls in or near the UV range. The laser-based bioprinting technique does not require a nozzle or orifice. It considers factors such as pulse frequency, laser energy, and the viscosity of the bioink used, among others.

3.3 Bioink

Since 2003, the term bioink has been introduced for organ printing, which refers to a cellular component placed in 3D on or within hydrogels²⁸. Nowadays, the term bioink refers to the composition of biomaterials and living cells that simulate the environment of the extracellular matrix, allowing cell adhesion, proliferation and differentiation after 3D bioprinting²¹.

Bioinks must have certain characteristics depending on the application. Therefore, it is important to consider biodegradability, biocompatibility, printability, mechanical integrity, stability, immunogenicity, toxicity and solubility in cell culture²¹. In bioink, the cells must be secured and protected against mechanical and thermal pressures. The mechanical properties help promote tissue regeneration, remodeling, and maturation. The bioink must achieve adequate solidification after printing to avoid nozzle blocking during slow printing speeds and to avoid structural failure of the bioprinted object due to layer weight accumulation during fast printing²⁹.

Bioinks can have several functions as support since they are applied to maintain cell populations and act as a synthetic extracellular matrix while cells grow. There are also fugitive bioinks, biomaterials that can leach, wash or dissolve in pores or channels within a printed structure. Bioinks possess structural characteristics that provide mechanical integrity to printed constructs. Finally, functional bioinks offer biochemical, mechanical or electrical signals that affect cellular performance after printing a structure²⁸.

Bioinks can be divided into two main types. The first type is scaffold-based, where cells are loaded into hydrogels or exogenous materials. Hydrogels facilitate tissue formation because they allow cell proliferation and growth. In a second type, the cells are bioprinted without using an exogenous biomaterial. The cells become neo-tissues that fuse and mature to produce functional tissues³⁰.

Bioink solutions used for bioprinting have been widely synthesized from polymers that are organic biomaterials possessing long chains with high water content. Thus, they can provide a hydrated tissue-like environment that supports cellular functions and tissue regeneration. The polymers are natural or synthetic. Natural polymers have the intrinsic ability to support cellular functions, while synthetic polymers are typically biologically inert but exhibit robust mechanical properties³¹. An adequate bioink must meet mechanical and structural properties be printable, biocompatible, among others. For this reason, most manufacturers of commercially available 3D bioprinters, especially those based on extrusion, recommend hydrogel bioinks³².

3.3.1 Hydrogel-based bioink

The hydrophilic functional groups in the monomeric unit can replenish the water absorbed in the 3D structure through hydrogen bonds³³. Water, along with growth factors and nutrients, can be supplied to the hydrogel scaffold to simulate the extracellular matrix environments of body tissue. Biocompatible hydrogels' chemical and mechanical properties can be precisely tuned to enable specific cellular interaction within printed cells, facilitating proliferation during tissue culture. Additionally, some hydrogels have cell-specific binding sites, facilitating cell adhesion, growth, and differentiation.

Hydrogels used in bioprinting can be divided into natural and synthetic categories. The most commonly mentioned natural hydrogels include collagen, fibrin, hyaluronic acid, alginate, agarose, chondroitin sulfate, matrigel, gelatin, and chitosan. Among these, collagen, fibrin, and gelatin contain intrinsic signals for cell adhesion. On the other hand, known synthetic hydrogels include poly(ethylene glycol) (PEG), Polycaprolactone (PCL), Poly(L-Lactic) Acid (PLA), Poly(vinyl alcohol) (PVA), and Poly(lactic-Co-Glycolic) Acid (PLGA)³³. Table 3.1 shows the advantages and disadvantages of the polymers mentioned. Natural hydrogels are the most used in tissue engineering applications due to their high bioactivity and similarities with extracellular matrix. However, due to their limited mechanical strength and rapid degradation, natural hydrogels alone are unsuitable for bioprinting. Therefore, hybrid bioinks combining natural and synthetic hydrogels have been developed to overcome these limitations in bioprinting.

3.3.2 Crosslinking of hydrogels

The hydrogel is a three-dimensional network that is hydrated in an aqueous medium. The connection between the chains of the hydrophilic polymer is called a network³³. Gelation is the process of cross-linking hydrogel molecules. At low to moderate concentrations, hydrophilic polymers behave like a Newtonian fluid. However, cross-linked molecules, known as hydrogels, exhibit viscoelasticity when in an aqueous solution. Hydrogels must have viscoelastic properties and gel quickly to be suitable for bioprinting. After bioprinting, each individually printed layer must be cross-linked to develop the structural and mechanical integrity of the printed construct. There are several cross-linking methods reported in the literature. Cross-linking of biodegradable and bioprintable hydrogels

Table 3.1: Advantages and disadvantages of materials used for 3D bioprinting.

Biomaterials	Advantages	Disadvantages	References
Alginate	<ul style="list-style-type: none"> - The viscosity is adjustable, changing the concentrations. - Crosslinking does not reduce cellular viability. - Compatible with a lot of cell types. - Rapid and easy crosslinking - Low cost - High cell viability pos printing 	<ul style="list-style-type: none"> - Low biodegradability - Poor mechanical strength - Low cell proliferation - Low cell recognition 	
Chitosan	<ul style="list-style-type: none"> - Good mechanical stability. - Easily to mix with other hydrogels. 	<ul style="list-style-type: none"> - Poor solubility - Low mechanical integrity - The solution requires neutralization because acids reduce cell viability. - It can be used alone 	
Collagen	<ul style="list-style-type: none"> - Good cell carrier - Easily to mix with other hydrogels - High biocompatibility 	<ul style="list-style-type: none"> - Low viscosity - Low mechanical integrity - Prolonged crosslinking time 	
Gelatin	<ul style="list-style-type: none"> - Thermoresponsive property - Good cell viability - Used as a cell carrier or fugitive bioink 	<ul style="list-style-type: none"> - Low viscosity - Low mechanical integrity - No stable at physiological temperature 	
Hyaluronic acid	<ul style="list-style-type: none"> - Good cellular carrier - Facilitate cellular proliferation - It is easy to modify - It can be mixed with other hydrogels 	<ul style="list-style-type: none"> - Low mechanical stability - No direct gelation - It can be used alone 	
Agarosa	<ul style="list-style-type: none"> - Provide good structural support in matrices 	<ul style="list-style-type: none"> - Non-biodegradable - Difficult bioprintability 	
Fibrin	<ul style="list-style-type: none"> - Promotes cell growth. 	<ul style="list-style-type: none"> - Liquefies at high temperature 	Kaliaraj et al. ³⁴
Matrigel	<ul style="list-style-type: none"> - High biocompatibility - Good environment for cell growth 	<ul style="list-style-type: none"> - Poor structural properties during printing - Requiere cooling for printing 	Fatimi et al. ³⁵ Lima et al. ³⁶ Tajic et al. ³⁷
Poly(ethylene glycol) (PEG)	<ul style="list-style-type: none"> - Easily to employ chemical characterization - Hydrophilic - Economical - Biocompatible - Easily combine with degradable materials 	<ul style="list-style-type: none"> - Nonbiodegradable - Low cellular proliferation - Photocrosslinking - Resistant to cell adhesion - Lacks mechanical strength 	Parodi et al. ⁹
Polycaprolactone (PCL)	<ul style="list-style-type: none"> - Biodegradable - Non-toxic - Hydrophobic - Low cost - Biocompatible 	<ul style="list-style-type: none"> - Bad prolonged half-life - Low bioactivity - Slow cell proliferation 	
Poly(L-Lactic) Acid (PLA)	<ul style="list-style-type: none"> - Biocompatible - Hydrolytical degradable 	<ul style="list-style-type: none"> - Material decomposition causes tissue inflammation and death in cells. 	
Poly(vinyl alcohol) (PVA)	<ul style="list-style-type: none"> - Water soluble - Biodegradable - Non-toxic - Chemical and mechanical stable - Good mechanical properties 	<ul style="list-style-type: none"> - Inadequate cell adhesion - Bad hydrophilicity 	
Poly(lactic-Co-Glycolic) Acid (PLGA)	<ul style="list-style-type: none"> - Biodegradable - Cytocompatibility - Hydrophobic 	<ul style="list-style-type: none"> - Fast disintegration 	

must be carried out under physiological conditions and can be driven by chemical (via covalent bonds), physical (reversible interactions), and enzymatic cross-linking³³.

Physical cross-linking is a gelation process in which polymer chains can be linked efficiently without forming covalent bonds.³⁸ Since this cross-linking occurs without chemical interactions and no external agent is used, the printed construct has no risk of cytotoxicity. Various mechanisms for this physical cross-linking are reported, such as ionic, hydrophobic, hydrophilic interaction, stereospecific and thermal self-assembly.

Ionic cross-linking arises from the electrostatic interaction between opposite charges. The bioink can be mixed with multivalent ions or an electrolyte solution with an opposite charge to the functional groups on the hydrogel chains. The combined ions can electrostatically attract the polymer chains and form a cross-linked hydrogel network. A well-known example is the ionic cross-linking of alginate in 3D printing, where alginate contains mannuronic and glucuronic acid in its polysaccharide chain and can form a hydrogel using calcium ions at room temperature and physiological pH³⁸.

Some hydrogels can physically gel through hydrophobic interactions or hydrogen bonds. This physical union depends on temperature and rheological changes. Some hydrogels show physical gelation at lower temperatures due to the ordered chain conformation, and upon heating, they show a random coil conformation. The hydrogel molecules form a cross-linked network at lower temperatures by hydrogen bonding with the absorbed water³³. These hydrogels are temperature sensitive and gel at physiological temperatures. There may also be stereospecific physical cross-linking, where oligomers with opposite chiralities couple with hydrophilic polymer chains to form hydrogels.

Chemical cross-linking involves covalent bonds between polymer molecules. Because these bonds are stronger than physical bonds, the printed structure should have higher mechanical strength after gelation. Exogenous chemical agents known as photoinitiators are added to carry out chemical cross-linking. These initiators, in the presence of photo radiation, form reactive free radicals by cleaving unimolecular bonds. These free radicals promote the formation of covalent bonds between two polymer chains at the point of unsaturation. However, photoinitiators can generate unwanted reaction products, leading to cytotoxicity and reduced cell viability. Researchers are working on developing biocompatible photoinitiators to overcome this problem. For 3D bioprinting, a UV curing head is used to cure each printed layer, with wavelengths of 365 nm or 405 nm being common. It is important to control the time of UV exposure during gelation to avoid damaging cellular DNA. There are several photoinitiators commercially available³⁸.

3.3.3 Requirements for bioink formulation

The bioink must possess optimal biological, physicochemical, rheological and mechanical properties³³. One of the crucial elements in using hydrogels for 3D bioprinting is the appropriate rheological parameters, which determine their printability. Most hydrogels show a decrease in viscosity under shear, which prevents nozzle clogging during the extrusion or inkjet process. Thinning hydrogels possess a high initial viscosity, resulting in high-fidelity printing of the structure. A suitable thinning hydrogel with the desired viscosity can maintain architectural integrity immediately after bioprinting.

The printability of bioink depends on various factors such as concentration, hydrophilicity, surface tension, the

self-crosslinking capacity of the hydrogel, cell density and surface properties of the printer nozzle³⁹. These, together with the viscosity of the hydrogel, determine the printing resolution, that is, the precise organization of the structure concerning the natural tissue. Furthermore, the dimension, shape, interconnection, and distribution of pores are critical to recreating an extracellular matrix-like microenvironment. The interconnection of pores facilitates the diffusion of oxygen, nutrients and metabolic products during cell proliferation⁴⁰.

The viscosity of the solution is influenced by the concentration of the hydrogel and the density of the encapsulated cells. A low solution viscosity improves printability but may result in lower mechanical stability of the printed structure. However, the higher the viscosity of the bioink, the higher the printing pressure needed for extrusion, which can decrease cell viability.

Cell viability in the printed bioink depends on the type and concentration of the hydrogel, cell-cell interactions, bioprinting modality, hydrogel degradation rate, and time after encapsulation. A low concentration of hydrogel favors cell proliferation, although mechanical properties and printing fidelity are better when the concentration is high. A highly concentrated hydrogel has a dense network of polymers, which hinders cell proliferation and migration. Furthermore, tissue regeneration can only take place with cell proliferation.

The cross-linking density in the hydrogel network is essential to determine the structural characteristics, mechanical properties, swelling index, and permeability to nutrients and metabolic products. As the cross-linking density increases, the spacing between macromolecular polymer chains decreases, improving the printed construct's mechanical strength⁴¹. However, the equilibrium swelling ratio and molecular diffusion are significantly reduced.

The bioink must have excellent cell adhesion properties in its characteristic chain sequence to facilitate the transfer of biomolecules and biochemical signals to the printed cells. Sometimes, it is necessary to modify the functional groups of polymer chains to create cell attachment sites and improve cell-hydrogel interactions. The biodegradation rate of the printed construct must match cell proliferation so that the cells' extracellular matrix (ECM) can replace the biodegradable construct⁴⁰. Furthermore, the biodegradable product resulting from degradation should not have a detrimental impact on the regenerated tissues. From a commercial perspective, bioinks are developed based on specific application requirements, which ensures that the properties of the hydrogel are compatible with those of the printed cell, enabling the creation of large-scale functional tissues. In addition to the abovementioned features, hydrogels must meet additional requirements such as industrial scalability, rapid availability, economic viability, and in vivo immunological compatibility³³.

3.3.4 Sodium alginate

Alginate is a usual linear polysaccharide biopolymer widely utilized in biomedical fields, like drug delivery, cell encapsulation, scaffolds, and 3D bioprinting⁴². Alginate is a biocompatible hydrogel that does not trigger an immune response. It shares similarities with the extracellular matrix and is well-suited for tissue regeneration. In addition to being cost-effective, alginate can be 3D printed into intricate and small structures with great accuracy¹³.

Alginates refer to calcium, magnesium, and sodium salts of alginic acid extracted from brown algae. Sodium alginate (SA), given by the formula $NaC_6H_7O_6$, is composed of two linked anionic monomers of 1,4- β -d-mannuronic and α -l-guluronic acids⁴³ as shows Figure 3.2. This polysaccharide is negatively charged, above the alginate's pKa

range of 3.4 and 4.4.

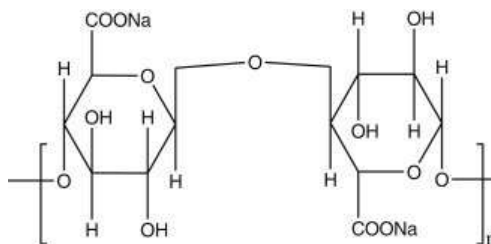


Figure 3.2: Chemical structure of sodium alginate. Adapted from Bhatia et al.⁴⁴

The capability of alginate to produce hydrogel by ionic crosslinking makes it popular. However, some modifications may be needed to promote its mechanical properties too⁷. Cross-linking by ionic interactions in alginate is carried out with physiological pH and at room temperature. It allows the alginate to encapsulate living cells and release proteins, creating a matrix. It is necessary to mention that cross-linked alginate gels can be destabilized by extracting calcium ions using a chelating agent.³⁸

When G residues are mixed with multivalent cations such as Ca^{2+} , they generate an ionic bridge between chains, and sodium alginate can be transformed into a hydrogel that retains more than 98% water⁴⁵. It is important to provide aqueous environments for the maintenance of bioactivity, and the entanglement of alginate chains form a three-dimensional net structure⁴⁶. In bioprinting, it is used because it supports cell growth and possesses high crosslinking ability and biocompatibility.

3.3.5 Gelatin

Gelatin is a biopolymer obtained by denaturing collagen, the main component of the extracellular matrix. Gelatin is a polypeptide comprising glycine, proline and 4-hydroxyproline residues⁴⁷ as Figure 3.3. Among the main characteristics of gelatin, it is soluble in water, it is biodegradable, and its main function is the integrity of the connective tissue, so it is possible to form biocompatible, biodegradable and non-immunogenic hydrogels when combined with other biomaterials. Other characteristics of this hydrogel are that it is economical compared to collagen and does not express antigenicity under physical conditions²⁰. Depending on the gelatin extraction method, it can be acidic or basic. Depending on this, its application varies.

Gelatin, similar to other proteins, exhibits optical activity in both its helical and random helical states. It is used as a gelling agent in the food, pharmaceutical and cosmetics industries and forms a gel when cooled below 35°C. These gelatin gels are clear, elastic, and can reverse when heated above 35°C. At lower temperatures, gelatin assumes a configuration similar to a collagen fold that allows the formation of hydrogen bonds between chains⁴⁷.

The gelling properties of gelatin can be modified by chemical cross-linking, an approach used by several researchers in the development of controlled release methods. Gelatin is a very valuable biopolymer in tissue engineering applications. However, its limitations in terms of mechanical properties restrict its use⁴⁸, and it is rarely

slower degradation of alginate-gelatin was observed in cell culture media, with a more than 60% decrease in initial modulus over seven days.

On the other hand, Bociaga et al.⁵¹ investigated the combination of sodium alginate and gelatin in different concentrations, analyzing the effect of various solvents on the mechanical and biological properties, as well as the extrusion capacity of the hydrogels. They concluded that adding gelatin (type B from bovine skin) to the alginate hydrogel increases the viscosity, regardless of the type of solvent. Likewise, the degradation rate was observed when the gelatin concentration increased.

Jia et al.⁵² developed alginate solutions with variations in oxidation and analyzed two crucial factors of bioink: viscosity and density. They modified cell attachment and spreading by conjugating RGD peptides to oxidized alginates. To avoid a high concentration of Ca^{2+} , they prepared a 100 mM $CaCl_2$ -gelatin solution with porcine gelatin (2% by weight). They adjusted the density of the bioink by varying the concentration and degree of oxidation, achieving a viscosity close to or higher than that of the cell type investigated, to obtain a homogeneous cell suspension.

3.5 Genipin crosslinking mechanism

Genipin (Gen), $C_{11}H_{14}O_5$, is an iridoid obtained by enzymatic hydrolysis of geniposide, the main active ingredient of the fruit of *Gardenia jasminoides*, which is a plant that belongs to the Rubiaceae family that grows wild in Vietnam, southern Vietnam, China, Taiwan, Japan, Myanmar and India. The figure shows that Gen comprises a dihydropyran ring and an ester group with a molecular weight of 226.226 g/mol and a melting point at a temperature of 120-121°C⁵³.

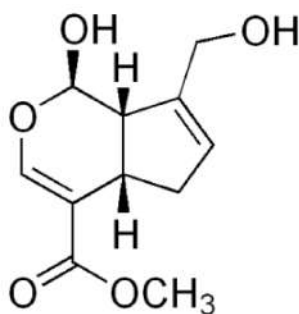


Figure 3.4: Chemical structure of genipin. Taken from Harris et al.⁵⁴

Gen is a white crystalline powder soluble in various solvents such as water, saline, acetone, ethyl acetate, propylene glycol and alcohol (methanol or ethanol). Under acidic and neutral conditions, it reacts spontaneously with the primary amines of the polymer chain, and the final product appears as dark blue pigments.

In recent years, Gen has attracted the attention of many researchers because it has cross-linking properties, and its toxicity is low. Therefore, the focus on its use and applications has expanded. For example, it can aid in wound healing through its anti-inflammatory and antioxidant properties, essential contributors to the healing cascade.

Gen reacts with primary and secondary amines. Gen, as a naturally-based cross-linking compound, stands out as the main method for manufacturing biomatrices. This approach seeks to overcome existing limitations and promises significant advances in wound healing in future clinical contexts. In addition, it confers a series of advantages to the resulting biomatrix, such as strengthening its mechanical resistance and toughness, reducing its solubility when exposed to enzymes and in liquid environments, conferring thermal stability and controlled expansion capacity, and improving its elasticity and viscosity⁵⁵.

Naturally derived cross-linking agents have been widely preferred for their ability to stabilize 3D scaffolds, promote biocompatibility, and low toxicity. Gen is 5,000 to 10,000 times less damaging to cells than other cross-linking substances, with a lethal dose 50 of approximately 200 mg/kg in the mouse model⁵⁶. The survival and proliferation rate of cells seeded in the biomatrix treated with Gen was 5,000 times higher than in the biomatrix treated with glutaraldehyde⁵⁷. Gen effectively inhibited inflammation and demonstrated an excellent biological safety profile following in vivo implantation studies.

Furthermore, the reactive capacity of Gen is subject to factors such as its concentration, cross-linking temperature, duration and critical pH determinants, which are reduced at low pH levels, thus allowing control over cross-linking density. The time required to carry out cross-linking is another critical indicator to ensure an appropriate balance between the manufacturing process and the retention of the desired shape⁵³.

Genipin has been used to manipulate various biomatrices derived from materials such as gelatin, chitosan, collagen, polyethylene glycol, hyaluronic acid, fibrin, and agarose, among others, due to its innate cross-linking capacity.

The exact mechanism of the genipin cross-linking reaction has yet to be fully understood. In this sense, several researchers have proposed that the genipin cross-linking process is carried out through the participation of two primary amino groups of the polymers, involving various routes and intermediates that give rise to a dimer product, which in turn induce the color change to blue in the solution. In general terms, the mechanism of this reaction is divided into two consecutive stages. The first involves the nucleophilic attack of an amino group on the polymer chain to the α,β -unsaturated ester in the genipin molecule, resulting in the opening of the genipin ring⁵⁷. Next, another amino group of the polymer chain will attack the methoxycarbonyl group, leading to an amide-type secondary bond and methanol release, forming the cross-linked compound⁵³. Figure 3.5 below illustrates the possible reaction that occurs during genipin cross-linking.

It has been suggested that the cross-linking reaction between gelatin and genipin occurs through two distinct pathways under slightly acidic or neutral conditions. The first reaction involves a nucleophilic attack of the amino groups on the gelatin ring to the genipin molecule's olefinic carbon atom (C3), followed by carbonyl and dihydropyran ring opening. Second, a nucleophilic attack of the amino groups of gelatin to the carboxyl group of genipin leads to amide formation. The further reaction involves an oxygen radical-induced genipin polymerization, which could occur between genipin molecules that have already been cross-linked with gelatin amino groups. It could result in genipin copolymers with high C=C conjugation. Furthermore, this phenomenon may be responsible for the bluish color observed in the gelatin scaffolds⁵⁸.

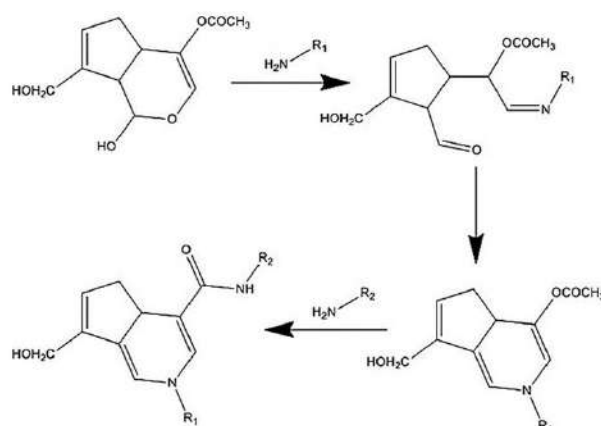


Figure 3.5: Crosslinking mechanism of Genipin. Taken from Utami et al.⁵³

3.6 Techniques of characterization and optimization of biomaterials

3.6.1 Fourier Transform Infrared spectroscopy (FT-IR)

Fourier Transform Infrared spectroscopy (FT-IR) is a technique that measures molecular vibrations induced by infrared radiation within a specific wavelength range. In this spectroscopic method, infrared radiation is directed through a sample. The sample absorbs infrared radiation while the rest passes through (transmits). The final spectrum represents the molecular absorption and transmission patterns, creating a unique molecular signature for the sample. The absorption peaks represent the vibration frequencies between the bonds of the atoms⁵⁹.

This technique furnishes valuable information, enabling researchers to identify unknown substances, assess the quality or uniformity of a sample, and ascertain the number of components in a mixture by analyzing the size of the peaks in the spectrum. Since each substance is a distinct arrangement of atoms, no two compounds yield precisely the same infrared spectrum⁶⁰.

An FT-IR equipment employs an interferometer shown in Figure 3.6 comprising a source, a beam splitter, a laser, a detector, and two mirrors. The energy emitted by the beam splitter divides the beam into two segments. One segment is directed towards a movable mirror, while the other is reflected towards a stationary mirror. The movable mirror oscillates back and forth at a consistent pace, regulated by the feedback from the calibration laser. The two beams are reflected off the mirrors, recombining at the beam splitter. Finally, it results in an interference pattern transmitted through the sample area to the detector. This signal is subsequently processed using the FT function to produce a spectrum. The resultant interference pattern, an interferogram, encompasses all information across all measured wavelengths. However, this signal must undergo a computationally intensive mathematical transformation, known as the Fourier transform, to yield an interpretable spectrum⁶¹.

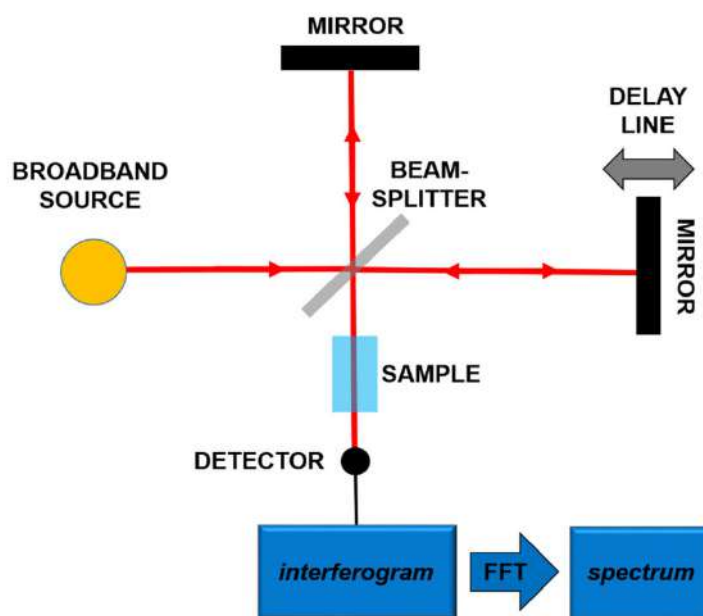


Figure 3.6: Principles of the Fourier-Transform Infrared Spectroscopy (FT-IR). Adapted from Patrizi et al.⁶²

3.6.2 Scanning electron microscope (SEM)

Scanning electron microscopy (SEM) is a technique used to analyze sample surfaces through the high-resolution images it produces. Figure 3.7 shows the design of an SEM, which comprises an electron gun, electromagnetic lenses, a vacuum chamber and detectors that collect the signals emitted from the specimen⁶³.

The SEM uses an electron source that generates a flow of accelerated charged particles toward the sample through a positive electric field. This electron beam is then restricted and concentrated through metal apertures and magnetic lenses, resulting in a narrow, focused, monochromatic beam. When these electrons collide with atoms in the sample, they cause the emission of signals that contain valuable information about the sample surface, including topographical details, composition, and electrical properties. These complex interactions and their effects are captured and translated into a visual image⁶⁴.

This tool can be applied to study topography, that is, the surface characteristics of an object and its texture⁶⁵. It is also possible to appreciate the morphology, which includes the shape and size of the particles that make up the object, the direct relationship between these structures and the properties of the materials. Finally, another application is to obtain the crystallographic information of how the atoms are arranged in the object⁶⁴.

In manufacturing hydrogels, exact knowledge of the microstructure, mainly its topology, is important. Therefore, cryogenic or high vacuum scanning electron microscopy is often used to visualize swollen hydrogels⁶⁶.

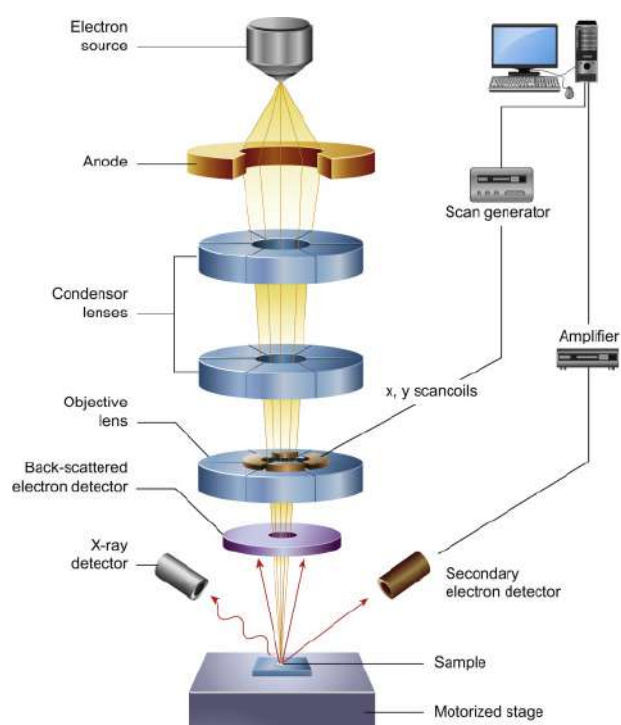


Figure 3.7: Diagram of components of SEM microscope. Adapted from Inkson B.J.⁶³

3.6.3 Biological characterization

Cell counting with trypan blue exclusion assay

The trypan blue assay was introduced, and to this day, it remains the most commonly used procedure to assess cell viability⁶⁷. The dye exclusion method assesses the quantity of viable cells within a cell suspension. This approach relies on the concept that viable cells maintain intact cell membranes that prevent the uptake of specific dyes like trypan blue, Eosin, or propidium, in contrast to non-viable cells⁶⁸(Figure 3.8).

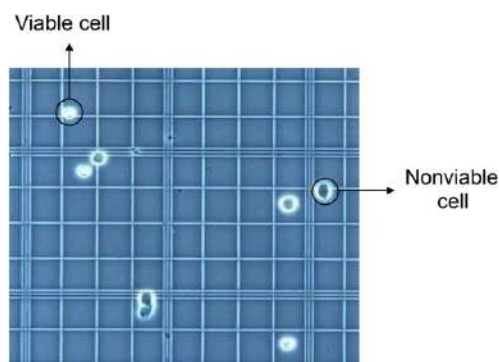


Figure 3.8: Trypan blue assay. Adapted from Kamiloglu et al.⁶⁹

After counting the cells, calculate the percentage of cell viability using the following formula:

$$\text{Viable cells (\%)} = \frac{\text{total number of viable cells per ml of aliquot}}{\text{total number of cells per ml of aliquot}} * 100$$

Cell viability by MTT assay

MTT is an assay to evaluate cell culture's viability and proliferation. The principle of this assay consists of measuring chemical biomarkers to evaluate the metabolic activity of the cells. So, the MTT assay converts the water-soluble yellow dye MTT to an insoluble purple formazan⁷⁰.

Over time, various tetrazolium salts have been created for different uses in areas such as histochemistry, cell biology, biochemistry, and biotechnology. In the field of cell cultures, MTT, XTT, MTS and WST stand out. Tetrazolium salt solutions are initially colorless or slightly discolored and become intensely colored as the formazan product is formed⁷¹.

Thus, the tetrazolium salt commonly used in cell cultures is MTT, introduced by Mosmann⁷² to evaluate proliferation and cytotoxicity in cultures, particularly in 96-well plate detection assays. Thanks to its lipophilic side groups and net positive charge, MTT can cross the cell membrane and be reduced in viable cells by mitochondrial or cell plasma enzymes, such as oxidoreductases, dehydrogenases, oxidases and peroxidases, which use electron donors such as NADH, NADPH, succinate or pyruvate. This process converts MTT to formazan (shown in Figure 3.9, a substance insoluble in water. In addition to enzymatic reactions, various non-enzymatic reactions with reducing

molecules, such as ascorbic acid, glutathione or coenzyme A, can interact with MTT to form formazan, increasing absorbance. The formation of needle-shaped formazan crystals damages cellular integrity and leads to cell death. It causes rapid disruption of the MTT reaction to formazan due to the metabolism breakdown. Since crystals form inside cells, MTT-based assay protocols typically include cell lysis and formazan dissolution steps before performing a spectroscopic measurement⁷³.

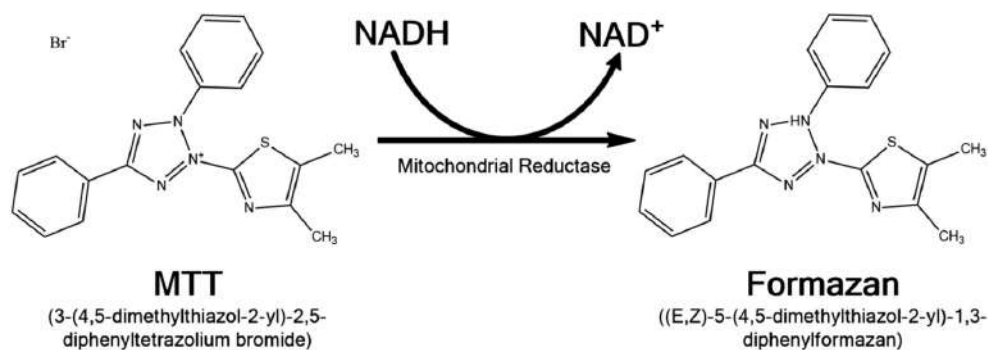


Figure 3.9: Reduction of MTT to formazan. Adapted from Kamiloglu et al.⁶⁹

3.7 Cell lines

3.7.1 Caco-2

The Caco-2 cell line originates from colon carcinoma and has been used as a model of the intestinal epithelial barrier⁷⁴. Initial investigations indicated that mature Caco-2 cells exhibited numerous structural and operational traits commonly found in enterocytes of the small intestine. Nevertheless, indicators associated with colon cells are also detectable within the Caco-2 cell population. Indeed, the Caco-2 model excels in foreseeing the permeability of compounds that pass through cells rather than the spaces between them. In typical circumstances, the permeability values for such transcellular compounds tend to be notably lower compared to the levels witnessed in live biological systems⁷⁵. These cells have morphological and functional properties of the small intestine's enterocytes⁷⁴. Therefore, they have been widely used to study intestinal physiology and as an intestinal barrier model to study toxicology in vitro. Reproducibility problems have been reported due to the variety of culture conditions related to the animal serum that used the supplements added, among other factors that make it difficult to compare laboratory results⁷⁶. This cell line has also been used in 3D bioprinting of tumor models, where the histological evaluation of Caco-2 cells has revealed the formation of glandular-type structures that show a greater pathomorphological resemblance to tumors than monolayer cultures⁴. Caco-2 cells are easy to identify because they form spheroids with a round structure similar to bubbles. In Figure 3.10 extracted from the work of Gheytanchi et al.⁷⁷, as he mentions, it can be observed in (d) The parental Caco-2 cells as a monolayer and (e), (f) The spheroids derived from Caco-2 showed a small and round morphology.

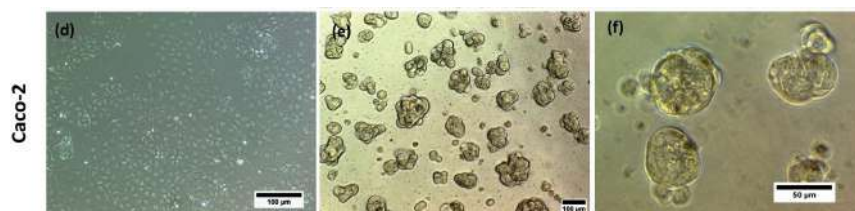


Figure 3.10: Morphology of Caco-2 cell line. Adapted from Gheyntanichi et al.⁷⁷

3.7.2 HUVEC

In 1973, researchers first described isolating human umbilical vein endothelial cells (HUVEC) because they discovered their use as a study model for cardiovascular diseases. HUVECs are obtained from umbilical cords formed in the fifth week of embryonic development⁷⁸.

The cell isolation process begins with collecting umbilical cords, which can be obtained from newborn babies naturally, from healthy mothers free of hepatitis or HIV. However, if it is necessary to study other pathologies, such as diabetes, the umbilical cords can be collected from mothers with said disease. After obtaining, correct conservation is necessary, so according to the literature, the optimal storage temperature is 4 degrees, and it is advisable to isolate the cells between 10 and 24 hours⁷⁸.

The isolation and cultivation process is described in the protocol established by Mari et al.⁷⁹ based on the isolation technique established by Jaffe et al.⁸⁰, who successfully isolated the cells for the first time and established the culture media considering morphological, immunohistological and serological criteria.

Regarding the morphology of HUVEC, it can be identified by their heterogeneity since they form a monolayer with a spiral pattern⁷⁸. The cells typically display uniformity, are elongated and polygonal, and have a centrally located oval nucleus. Next, Figure 3.11 shows the different morphology of the confluent HUVEC cells with an elongated shape and the non-confluent cells with a spherical shape⁸¹.

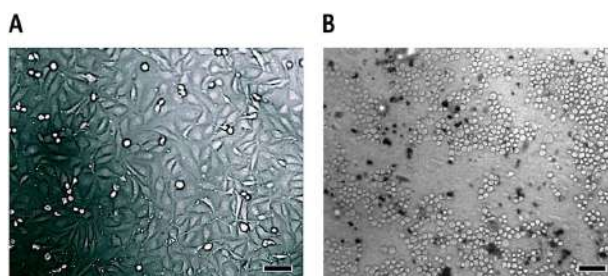


Figure 3.11: Morphology of HUVEC cell line. Retrieved from Urbaczek et al.⁸¹

Chapter 4

Methodology

4.1 Synthesis of bioinks

4.1.1 Hydrogel preparation

Hydrogels were prepared using natural polymers such as gelatin (G) and sodium alginate (SA) in different proportions and concentrations. Figure 4.1 shows the setup to prepare hydrogels.



Figure 4.1: Setup of hydrogel preparation.

Two solvents were used to prepare hydrogels: distilled water and DPBS (Dulbecco's Phosphate Buffered Saline, with $MgCl_2$ and $CaCl_2$, liquid, sterile-filtered).

First, in distilled water, the sodium alginate (Alquimia, Farmácia de manipulação, São Paulo, Brazil) was dissolved at two different concentrations of 3.6 and 6 % (w/v) using a magnetic stirrer at 50°C for 16 hours, while gelatin (Didática SP, Brazil) was prepared at 1 and 5 % (w/v) at 50°C with stirring for 18 hours. The obtained

solutions of alginate and gelatin were mixed with different proportions to form composite hydrogels using a magnetic stirrer for homogenizing the solutions. A 20 mM $CaCl_2$ (Alquimia, Farmácia de manipulação, São Paulo, Brazil) solution was prepared for the crosslinking of SA. Then, in a proportion of (1:1) was mixed SA 3.6% (w/v) and $CaCl_2$, and alginate 6% (w/v) and $CaCl_2$. Also, the composite hydrogels were mixed with the $CaCl_2$ solution in the proportion of (1:1:1) for the cross-linking.

Another crosslinking agent used was genipin (Gen) $\geq 98\%$ (HPLC), powder (Sigma-Aldrich, Brazil). A stock solution at a concentration of 1.66% (w/v) was prepared in ethanol 100%. Then, SA was combined with genipin added from the solution stock to obtain concentrations of 0.25, 0.5, and 1 % (v/v) (Figure 4.2).



Figure 4.2: Sodium alginate crosslinking with genipin at concentrations of 0.25, 0.5, and 1 % (v/v) (left to right).

The composite hydrogels were also crosslinked with genipin at the same concentrations (Figure 4.3).



Figure 4.3: Hydrogels composites crosslinking with genipin at concentrations of 1, 0.5, and 0.25% (v/v) (left to right).

DPBS was used as a second solvent to solve gelatin 1 and 5 % (w/v) and alginate 3.6% (w/v) with agitation at 50°C for 16 hours. Then, using stirring to homogenize the solutions, composite hydrogels were prepared with different proportions.

Table 4.1 presents the numeration, abbreviations, concentrations, proportions and the individual composition of the samples used for each assay.

Table 4.1: Compositions of hydrogels.

Sample number	Abbreviations	Concentration				Proportions	Solvent
		Sodium alginate (% w/v)	Gelatin (% w/v)	Genipin (% v/v)	CaCl ₂ (mM)		
1	G 1%	-	1	-	-	-	DPBS
2	SA 3.6%	3.6	-	-	-	-	water
3	SA 3.6% + CaCl ₂	3.6	-	-	20	(1:1)	water
4	SA 3.6% + G 1% + CaCl ₂	3.6	1	-	20	(1:1:1)	water
5	SA 3.6%	3.6	-	-	-	-	DPBS
6	SA 3.6% + G 5%	3.6	5	-	-	(2:1)	DPBS
7	SA 6% + CaCl ₂	6	-	-	20	(1:1)	water
8	SA 3.6% + G 5% + CaCl ₂	3.6	5	-	20	(1:1:1)	water
9	SA 3.6% + G 1%	3.6	1	-	-	(1:1)	DPBS
10	SA 3.6% + G 5%	3.6	5	-	-	(1:1)	DPBS
11	SA 3.6% + G 1%	3.6	1	-	-	(2:1)	DPBS
12	SA 3.6% + G 5% + Gen 1%	3.6	5	1	-	(1:1)	water
13	SA 3.6% + G 5% + Gen 0.25%	3.6	5	0.25	-	(1:1)	water
14	SA 3.6% + Gen 0.25%	3.6	-	0.25	-		water
15	SA 3.6% + Gen 1%	3.6	-	1	-		water
16	SA 3.6% + Gen 0.5%	3.6	-	0.5	-		water
17	SA 3.6% + G 5% + Gen 0.5%	3.6	5	0.5	-	(1:1)	water
18	G 1%	-	1	-	-	-	water

4.2 Characterization

4.2.1 FT-IR spectroscopy

The FT-IR spectra were taken with an FT-IR Spectrometer Bruker Optik GmbH Tensor 27. This apparatus belongs to the São Carlos Institute of Chemistry of the University of São Paulo. The principle of this equipment worked only by measuring a drop of the sample, which had been calibrated before with a drop of distilled water. In Figure 4.4, a picture of the equipment used.



Figure 4.4: FT-IR Spectrometer Bruker Optik GmbH Tensor 27.

4.2.2 SEM

The hydrogel samples were frozen at -80°C for 6 hours. Then, the samples were freeze-dried using the benchtop freeze dryer LS 3000 Terroni, shown in Figure 4.5, for 24 hours before the metalization for the characterization.



Figure 4.5: Benchtop freeze dryer LS 3000 Terroni.

The cross-sectional surface of the sliced hydrogels was observed under a scanning electron microscope (SEM) to study the surface morphology. SEM images were acquired at 100X, 500 X and 1000 X magnifications using LEO

model 440 Scanning Electron Microscope at 15 kV (Figure 4.6). The equipment mentioned in this section belongs to the São Carlos Institute of Chemistry of the University of São Paulo.



Figure 4.6: LEO model 440 Scanning Electron Microscope.

4.3 Cell culture

4.3.1 Culture conditions for Caco-2

The human colorectal adenocarcinoma epithelial cell (colorectal adenocarcinoma cell - CaCo-2) is an immortalized cell obtained from the American Type Culture Cell (ATCC® HTB-37™) collection. These cells were grown in polystyrene cell culture flasks (Corning®) with high glucose modified Eagle's medium (DMEM, Gibco™), supplemented with 10% fetal bovine serum (SFB, Vitrocell embryolife®), 1.0% of penicillin/streptomycin (Vitrocell embryolife®) and 1.0% non-essential amino acids (Gibco™). Cells were maintained in a 5.0% CO_2 incubator (PHCbi IncuSafe CO_2 Laboratory Incubator) at 37°C. Caco-2 was grown in passages 38-50.

4.3.2 Culture conditions for HUVEC

Endothelial cells from the human umbilical cord vein (Human Umbilical Vein Endothelial Cell - HUVEC, CRL-2873™ ATCC®) were cultured in 25 cm^2 and 75 cm^2 polystyrene flasks (Corning®) with Roswell Park Memorial Institute Medium 1640 (RPMI, Sigma-Aldrich®) supplemented with 10% FBS, 25 mM HEPES (Sigma-Aldrich®), and 1.0% penicillin/streptomycin mixture. Cells were maintained at 37°C in a humidified 5.0% CO_2 incubator and recultured (2.0×10^5 cells. mL^{-1}) at passages 40-50.

4.4 Cell viability

4.4.1 Trypan blue exclusion assay

After cell culture, viable cell counting was performed. An aliquot was centrifuged from the cell suspension for 5 minutes, and the supernatant was discarded. The cell's pellet was resuspended in a serum-free complete medium. A dilution of cells was prepared by mixing trypan blue. Then, to make the count of cells, a drop of the trypan blue/cell mixture was applied to a Neubauer chamber, which was placed on the stage of an optical microscopy microscope and focused on the cell to distinguish between the unstained (viable) and stained (nonviable) cells (Figure 4.7).

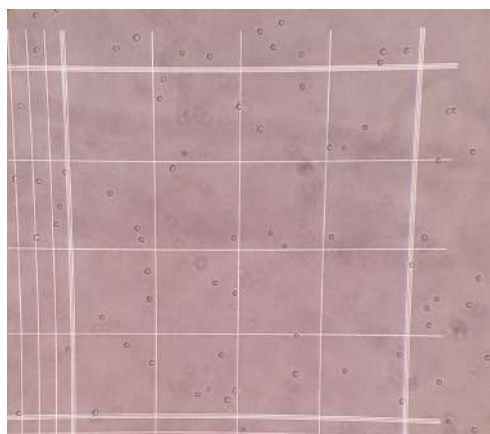


Figure 4.7: Caco-2 cells with trypan blue in the Neubauer chamber.

To calculate viable cells per ml of the sample, after counting the viable and nonviable cells, multiply the total count of viable cells by 2, which accounts for the trypan blue dilution factor. To determine the overall cell count per ml of the sample, sum up the total counts of viable and nonviable cells and then multiply the sum by 2. Finally, was calculated the percentage of viable cells. This process was made for the two cell lines.

Caco-2

- Living cells: 495
- Dead cells: 17

$$\text{Viable cells (\%)} = \frac{\text{total number of viable cells per ml of aliquot}}{\text{total number of cells per ml of aliquot}} * 100$$

$$\text{Viable cells (\%)} = \frac{990}{1024} * 100$$

$$\text{Viable cells (\%)} = 96.68\%$$

HUVEC

- Living cells: 272
- Dead cells: 12

$$\text{Viable cells (\%)} = \frac{\text{total number of viable cells per ml of aliquot}}{\text{total number of cells per ml of aliquot}} * 100$$

$$\text{Viable cells (\%)} = \frac{544}{568} * 100$$

$$\text{Viable cells (\%)} = 95.77\%$$

4.4.2 MTT assay for hydrogels

In this assay, the negative control (C-) was the respective cell culture media, and the positive control (C+) was a 2.0 cm^2 cutout from a surgical glove (Medfeel) that was immersed in the culture medium for 24 h. HUVEC, Caco-2 cells were cultivated in a 96-well plate (NEST®) (1.0×10^5 cells. mL^{-1}) in sextuplicate and maintained for 48h in an incubator at 5.0% CO_2 and 37°C. After 24h, the hydrogels were introduced into microplates under cell culture (Figure 4.8) that remained in an incubator at 5.0% CO_2 and 37 °C for 12h. Then, 1.0 mg. mL^{-1} of the methyl thiazolyl tetrazolium (MTT) assay kit was added for 3 hours in an incubator at 5% CO_2 and 37°C. The formed formazan was dissolved in 200 μ L of DMSO.



Figure 4.8: Cells cultivated in hydrogels on a 96-well plate.

Then, absorbance was measured using the 550 nm filter for HUVEC cells and the 570 nm filter for Caco-2 cells in a spectrophotometer Thermo Scientific™ Varioskan™ LUX multimode microplate reader (Figure 4.9). This apparatus belongs to the São Carlos Institute of Chemistry of the University of São Paulo.



Figure 4.9: Thermo Scientific™ Varioskan™ LUX multimode microplate reader.

Before applying the MTT assay kit, micrographs were taken with the OLYMPUS Q-Color 5™ camera of the Olympus CKX41 Inverted Microscope (Figure 4.10) using the software Olympus cellSens Standard. Equipment from the São Carlos Institute of Chemistry of the University of São Paulo.



Figure 4.10: Olympus CKX41 Inverted Microscope.

The calculation of the survival index – IS (%) was carried out in relation to the negative control, which represents an absorbance of 100% cell viability, as shown in the following equation.

$$IS (\%) = \frac{X_{average}}{C(-)_{average}} \times 100$$

Where $X_{average}$ is the mean absorbance of each sample, and $C(-)_{average}$ is the mean absorbance of the negative control.

Statistics

The quantitative data is presented as means with standard deviation. Statistical analysis was conducted using one-way ANOVA followed by a post hoc Dunnett test with GraphPad Prism version 10. In the figures, "*****" in the legend indicates $p < 0.0001$, "****" represents $p < 0.001$, "***" represents $p < 0.01$, "**" represents $p < 0.05$, and "ns" indicates non-significant.

Chapter 5

Results & Discussion

5.1 FT-IR spectroscopy

The spectral behavior of alginate, gelatin, composites of gelatin and alginate, $CaCl_2$, DPBS, and genipin are illustrated in the following figures.

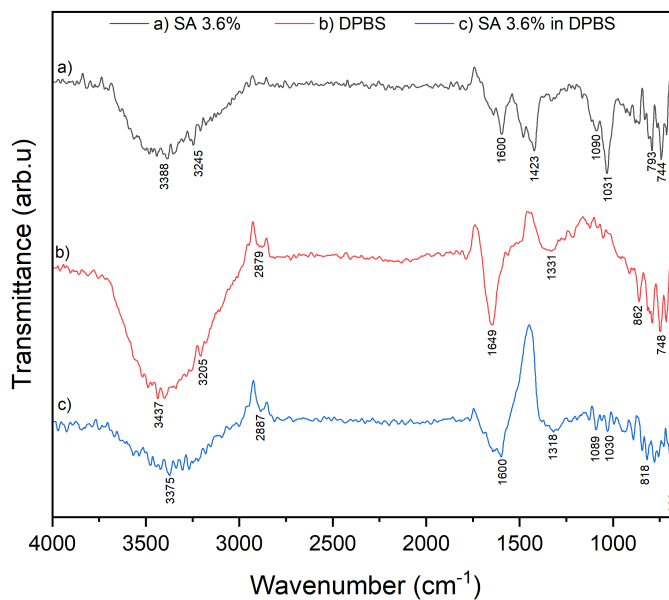


Figure 5.1: FT-IR spectra of a) sodium alginate 3.6%, b) DPBS, and c) sodium alginate 3.6% solved in DPBS.

First, in Figure 5.1, curve a) shows the spectra of sodium alginate solved in distilled water at a concentration of 3.6%. The broad band at wavenumber 3388 cm^{-1} is attributed to the O-H functional group⁸². The characteristic peaks at 1600 and 1423 cm^{-1} are assigned to the vibrations of COO^- for the carboxyl group of sodium alginate. Moreover, the peak at the wavenumbers 1090 and 1031 cm^{-1} are attributed to the C-O and C-O-C stretching vibrations of the saccharide structure⁸³. Finally, the wavenumber 793 and 744 cm^{-1} showed in the spectrum is related to mannuronic and guluronic acid residues, respectively⁸⁴.

In curve b), the DPBS spectro is shown, and it presents bands at 3437 cm^{-1} of the O-H group, at 2879 cm^{-1} of C-H, and 1649 cm^{-1} of C=O. Also, curve c) shows the spectra of sodium alginate, but solved in DPBS, it is possible to identify the characteristic groups of alginate. The band is the O-H functional group at 3375 cm^{-1} . The vibration of $-\text{COO}^-$ for the carboxyl group at 1600 cm^{-1} . wavenumber 1031 cm^{-1} of C-O-C stretching vibrations of the saccharide structure.

If the spectra of the alginate dissolved in water were compared with the alginate dissolved in DPBS, it could be observed that there is a slight modification in the peaks, which is attributed to the composition of the DPBS because it contains MgCl_2 and CaCl_2 and according to the literature, Ca ions bind to Mg and generate the crosslinking of sodium alginate⁸⁵. Among the changes that can be observed, the shifting and shortening of the peaks are wave numbers 1318, 1089, and 1030 cm^{-1} ⁸⁶.

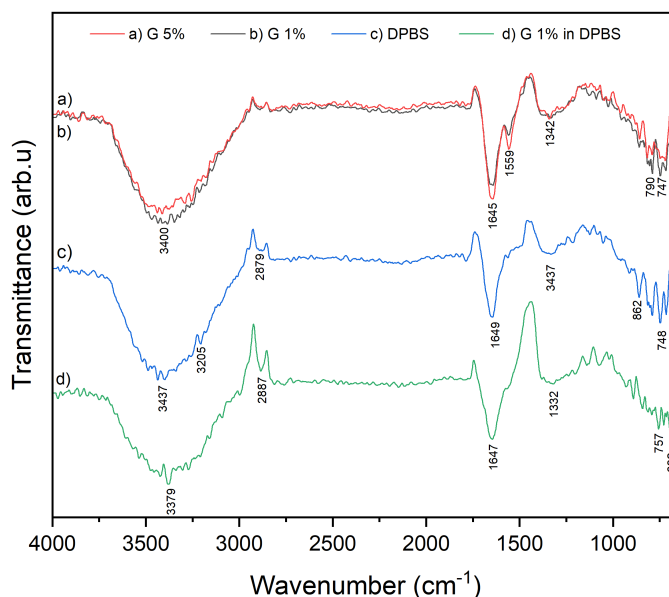


Figure 5.2: FT-IR spectra of a) gelatin 5%, b) gelatin 1%, c) DPBS, and d) gelatin 1% solved in DPBS.

In Figure 5.2, curves a) and b) show the FT-IR spectra for gelatin solved in distilled water at concentrations of

5 and 1 %, respectively. Gelatin 1% and 5% showed vibration peaks at the wavenumbers of 3400cm^{-1} attributed to the presence of hydrogen bond water, 1645cm^{-1} peak corresponds to Amide I that represents C=O stretching of peptide bonds of gelatin, at 1559cm^{-1} indicate Amide II which represents the bending vibration of N-H groups and stretching vibrations of C-N groups⁸⁷, band at 1342cm^{-1} correspond to amide III, which is related to the vibrations in the plane of C-N and N-H groups of bound amide⁸⁸. On the other hand, gelatin 1% prepared with DPBS has a similar spectro, but some bands in 1645 have elongation, and the peak of 1553cm^{-1} disappears due to the interaction with the solvent component¹⁵.

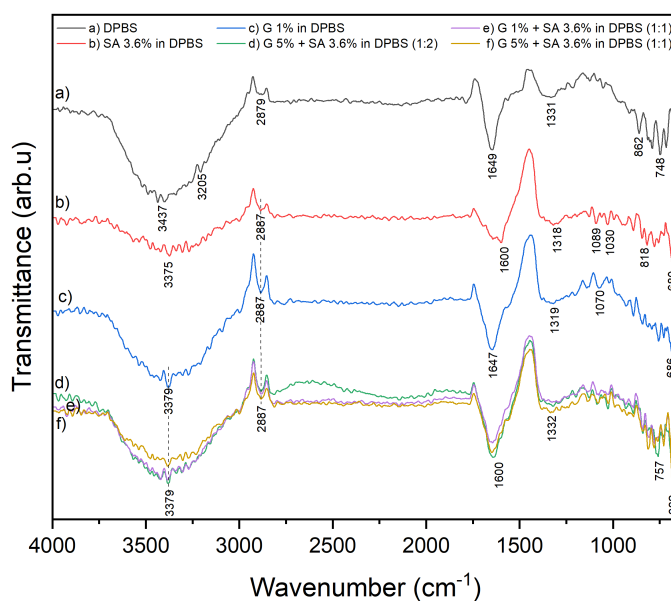


Figure 5.3: FT-IR spectra of a) DPBS, b) sodium alginate 3.6% solved in DPBS, gelatin 5% solved in DPBS, and composites of alginate with gelatin solved in DPBS at different concentrations.

The gelatin and sodium alginate spectra composites prepared at different concentrations are shown in curves d), e), and f) of Figure 5.3. The band of 1600cm^{-1} corresponds to Amide I for gelatin, and the absorption at 1332cm^{-1} is assigned to stretching vibration of COO^- has shifted to the lower number respect with the pure polymers. According to Derkach, S. et al., these alterations suggest the development of robust intermolecular connections, encompassing hydrogen bonding and electrostatic attractions, between sodium alginate and gelatin chains, leading to the self-assembly of polyelectrolyte complexes⁸⁹.

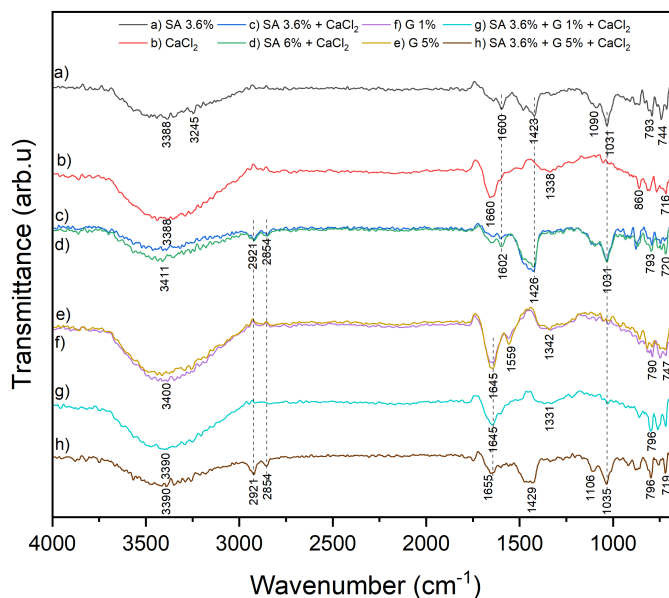


Figure 5.4: FT-IR spectra of a) SA 3.6%, b) $CaCl_2$, c) SA 3.6% + $CaCl_2$, d) SA 6% + $CaCl_2$, e) G 5%, f) G 1%, g) SA 3.6% + G1% + $CaCl_2$, and h) g) SA 3.6% + G5% + $CaCl_2$

Figure 5.4 shows the spectra corresponding to b) $CaCl_2$ solution. At wavenumber 3388cm^{-1} , the vibrations of the O-H connections are visualized due to the presence of water in the solution. At 1660cm^{-1} , the vibrations of the H-O-H bending due to the water. The peaks at 1338 , 880 , and 716cm^{-1} are associated with calcium and oxygen links or the flexion and torsion of bonds between the atoms, such as calcium and chlorine⁹⁰.

Curves c) and d) show the spectra of alginate 3.6% + $CaCl_2$ and alginate 6% + $CaCl_2$, respectively. If they are compared with the spectra of alginate, it is possible to observe two characteristic peaks at wavenumber 2921 and 2854cm^{-1} linked to the C-H stretching bond appear. The peak at 1602 and 1426cm^{-1} are attributed to the asymmetric and symmetric stretching vibration of the COO^- group.

The cross-linking of sodium alginate by a concentration of Ca^{2+} from $CaCl_2$ can be demonstrated by a reduction in intensity and a slight modification in the wave number of the peak of the carbonyl group due to the replacement of sodium ions by calcium ions calcium⁹¹. For this reason, the peaks of pure alginate are at 1602 and 1426cm^{-1} instead of 1600 and 1423cm^{-1} . The C-C peak that extends to 1031cm^{-1} due to its intensity suggests a stronger O-H bonding vibration or a stronger binding of Ca^{2+} to the guluronic acids of sodium alginate⁹².

Finally, spectra h) and g) of alginate with gelatin and $CaCl_2$ mixtures show significant changes. The Amid I band at 1645cm^{-1} for gelatin has been coupled with the strong absorption band at 1600cm^{-1} for SA assigned to the asymmetric stretching vibration of the COO^- and has moved to a higher wave number when the gelatin concentration

increases (1655cm^{-1}) and is maintained when the concentration is 1% (1645cm^{-1}). At the same time, the absorption at 1423cm^{-1} assigned to the symmetric stretching vibration of the COO^- has moved to the lowest wave number (1331cm^{-1}) when the gelatin concentration is 1%. However, when it is 5%, it increases to 1429cm^{-1} . According to the literature, these changes imply the formation of strong intermolecular interactions, including hydrogen bonds and electrostatic attractions between sodium alginate and gelatin chains, with the self-organization of polyelectrolyte complexes²⁶.

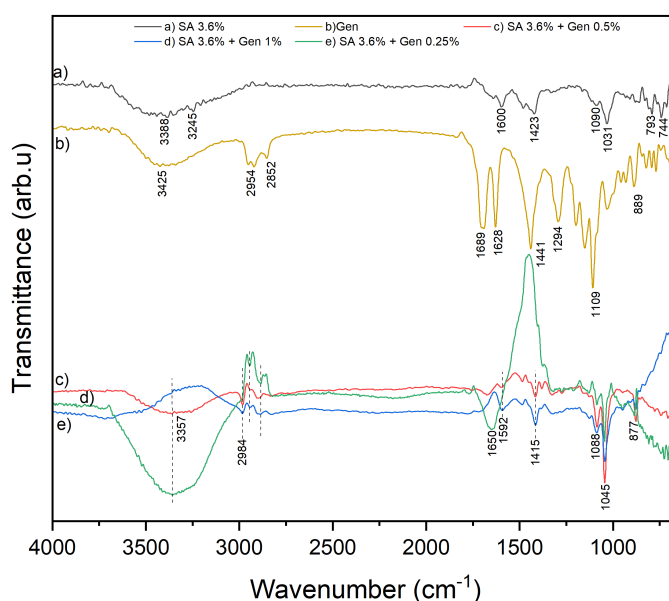


Figure 5.5: FT-IR spectra of a) SA 3.6%, b) Gen, c) SA 3.6% + Gen 0.5%, d) SA 6% + Gen 1%, e) SA 6% + Gen 0.25%.

In Figure 5.5, spectra b) correspond to the genipin solution. The characteristic peaks are observed at 1689cm^{-1} and 1628cm^{-1} , which correspond to the $\text{C}=\text{C}$ stretching of the carboxymethyl group and aromatic stretching⁹³. Genipin also indicated peaks at 3413cm^{-1} ($-\text{OH}$ stretching vibration), 2954 and 2852cm^{-1} ($\text{C}-\text{H}$ stretching vibrations), 1441cm^{-1} (CH_3 bend of the methyl ester), 1294cm^{-1} ($\text{C}-\text{O}-\text{C}$ asymmetric stretch), and 1109cm^{-1} ($\text{C}-\text{O}-\text{C}$ stretching vibrations). Finally, the band at 889cm^{-1} correspond to the $\text{C}-\text{H}$ ring out-of-plane bend⁹⁴.

In c), d), and e) have a mix of alginate with genipin at different concentrations. c) has a concentration of genipin of 0.5%, and the characteristic peaks of sodium alginate are at 1592 and 1425cm^{-1} . They are moving in relation to pure sodium alginate, and it can be an indicator of cross-linking. Moreover, at wavenumber 3357cm^{-1} , the vibrations of the $\text{O}-\text{H}$ and other peaks take place at 1088cm^{-1} of mannuronic units, 1045cm^{-1} attributed to guluronic units and 877cm^{-1} of saccharide structure. Curve d), in which the genipin has a concentration of 0.25%, shows a band

at wavenumber 3357cm^{-1} but much broader and possesses equal peaks of c). However, e) resents different bands at the wavelength 1650 attributed to C=O and 1045 of the guluronic residues.

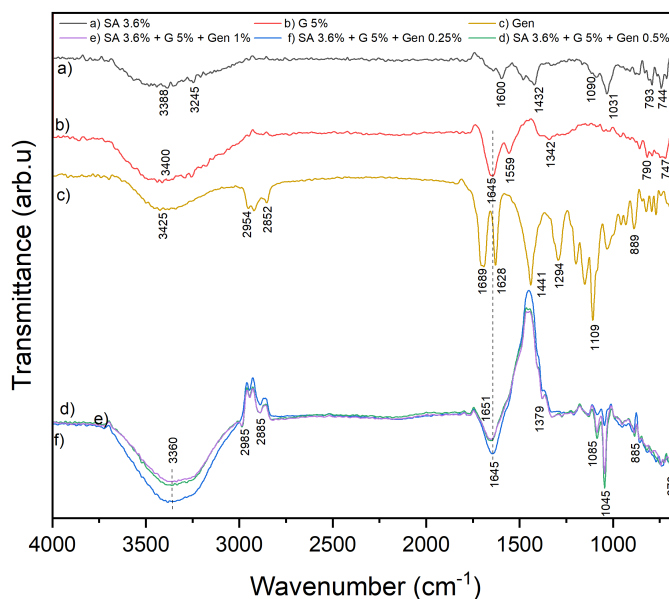


Figure 5.6: FT-IR spectra of a) SA 3.6%, b) G 5%, c) Gen, d) SA 3.6% + G 5% + Gen 0.5%, d) SA 6% + G 5% + Gen 1%, e) SA 6% + G 5% + Gen 0.25%.

Figure 5.6 shows the spectra of alginate 3.6% and gelatin 5% with different genipin concentrations. It is possible to observe characteristic peaks at 3360cm^{-1} of the O-H functional group, 2985 and 2885cm^{-1} attributed to N-H, 1646cm^{-1} which is the Amida I. This band could indicate cross-linking with genipin because, according to the cross-linking mechanism, the polymeric amino group found in gelatin undergoes a nucleophilic attack on the olefinic carbon atom of genipin. Other values, such as 1379cm^{-1} , had a displacement concerning the gelatin and alginate. Finally, other peaks at 1045cm^{-1} correspond to the guluronic units.

5.2 Morphology of hydrogels

In this section, the structure of the hydrogels prepared with different compositions is visualized by SEM in different magnifications.

Figure 5.7 shows the microstructure of a hydrogel composed of SA, G and CaCl_2 . The surface of these hydrogels is very porous, the size of the pores is random, and the walls' thickness is medium, which is characteristic of alginate

and gelatin hydrogels crosslinked $CaCl_2$ so that cells can lodge⁹⁵.

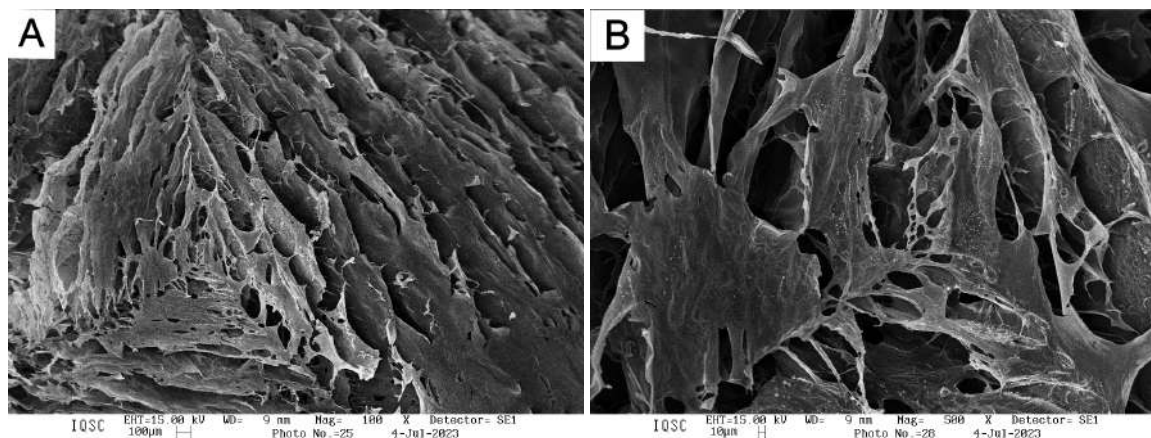


Figure 5.7: SEM microphotographs of hydrogel formed of SA 3.6% + G 5% + $CaCl_2$ at different magnifications A) 100X, B) 500X.

Next, the hydrogels composed of SA and G that were solved in DPBS (Figure 5.8) show that the structure is porous, and with the magnification of the image, notice that the thickness of the walls is great; in some places, the wall is smooth, and in others, it is irregular.

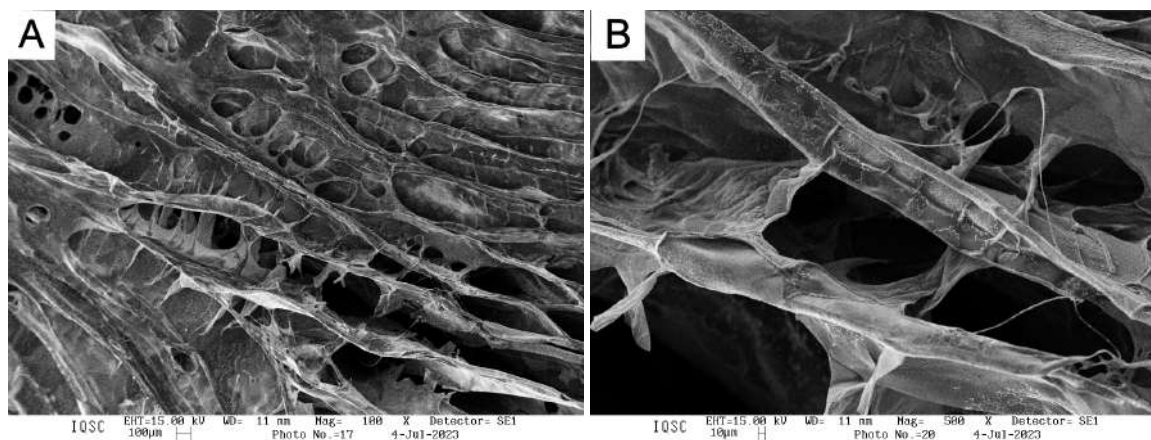


Figure 5.8: SEM microphotographs of hydrogel formed of SA 3.6% + G 1% in PBS (2:1) at different magnifications A) 100X, B) 500X.

Figure 5.9 shows that the structure is much more porous than the previous one. This is because the gelatin concentration is much higher than the hydrogel composition described above. The size of the pores is somewhat varied, but smaller pores predominate. The walls also have a smaller thickness.

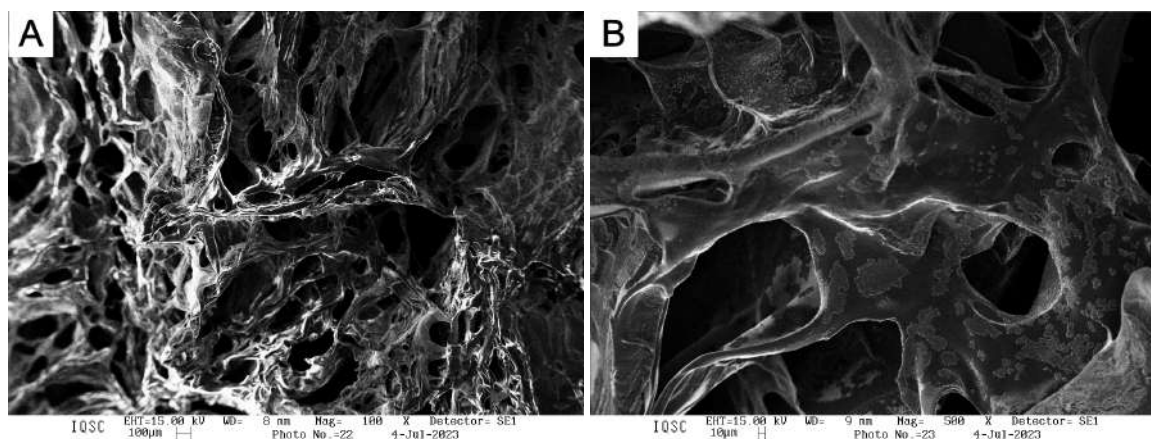


Figure 5.9: SEM microphotographs of hydrogel formed of SA 3.6% + G 5% in PBS (2:1) at different magnifications A) 100X, B) 500X.

The microstructure of the hydrogel formed by SA, G, and Gen (Figure 5.10) is not shown uniformly throughout the image since a porous structure with a moderately regular size is shown in the upper right image. With zoom-in on the image at 500X, it can be seen that the internal structure is also porous, and the walls are thin. However, the surface of the walls is not completely smooth but has smaller pores, as seen in C.

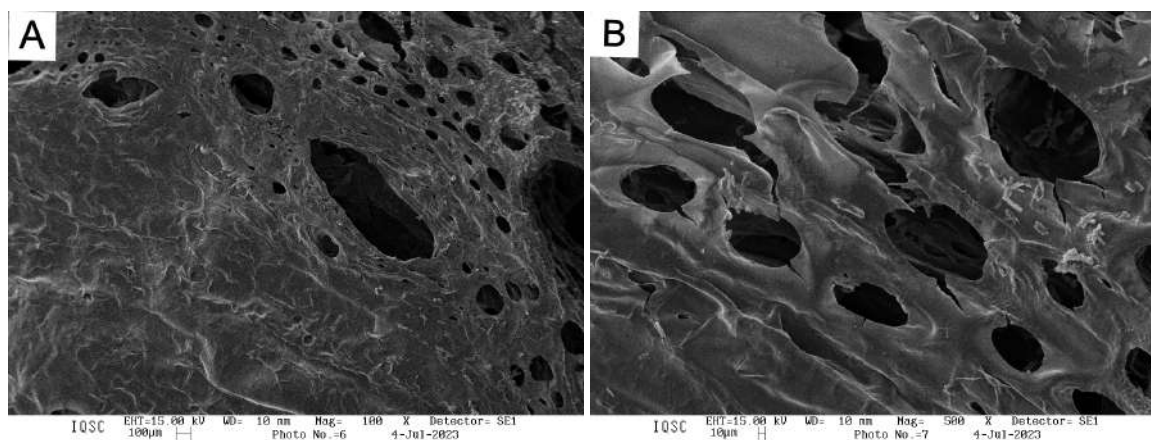


Figure 5.10: SEM microphotographs of a film of hydrogel formed of SA 3.6% + G 5% + Gen 0.5% at different magnifications A) 100X, B) 500X.

The structure in Figure 5.11 corresponds to a composition of SA with Gen at a concentration of 1%, and it can be seen that the structure is highly porous. The structure is elongated and of similar size. In C, it is possible to see that the walls are smooth.

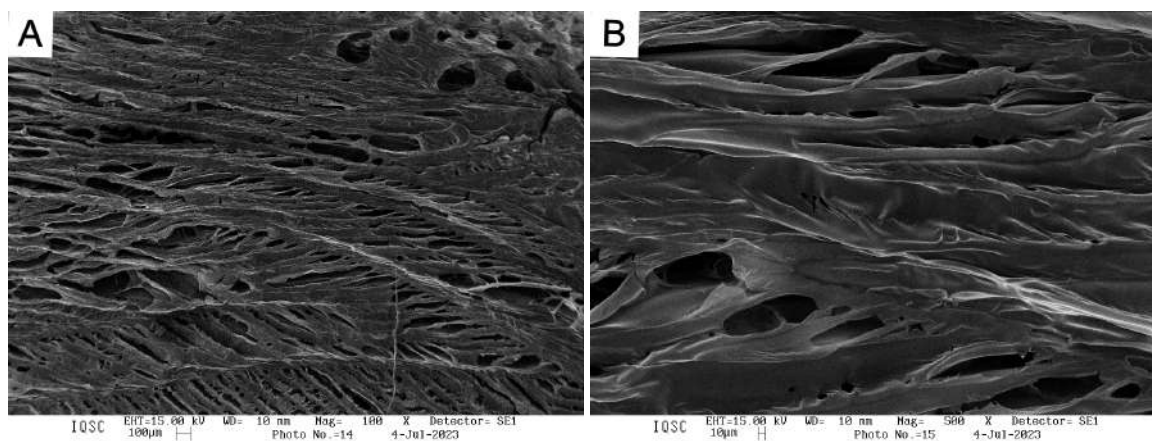


Figure 5.11: SEM microphotographs of hydrogel formed of SA 3.6% + Gen 1% at different magnifications A) 100X, B) 500X.

Finally, this Figure 5.12 is of a hydrogel with the same composition as the previous one, but this went through a temperature change. The surface is non-porous and shows smooth walls. However, when the magnification increases, very small pores and some residues can be observed on the surface.

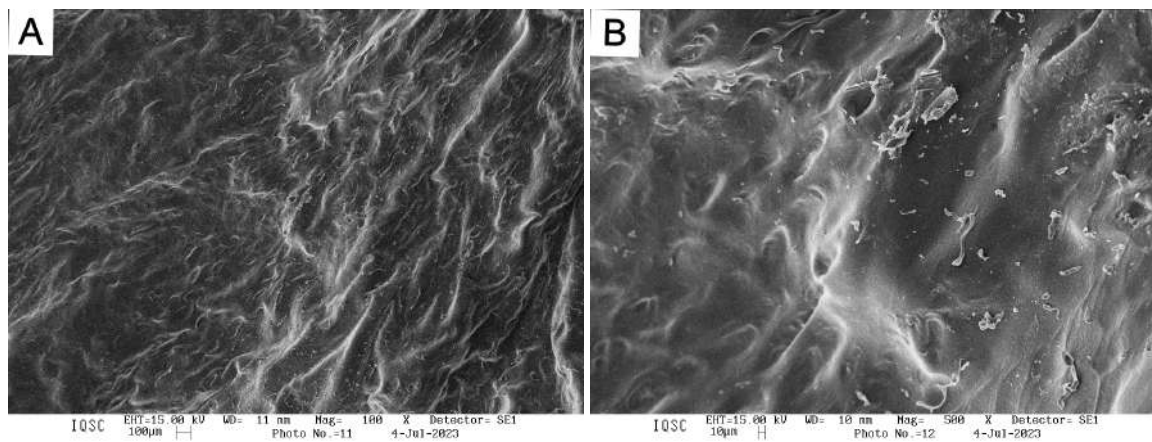


Figure 5.12: SEM microphotographs of hydrogel formed of SA 3.6% + Gen 0.25% at different magnifications A) 100X, B) 500X.

5.3 Cell viability of alginate and gelatin hydrogels

This section presents the statistical results of the MTT assay, where the absorbance was read at a wavelength of 550 nm for HUVEC and 570 nm for Caco-2. The results were compared to the negative control with One-way ANOVA followed by post hoc Dunnett test. The statistical difference between the viability of cells seeded on the hydrogels and the control is shown with the asterisks.

So, according to the MTT assay, the percentage of cell viability and proliferation corresponding to the positive and negative controls of the HUVEC cell line are 14.48% and 91.70%, respectively. For the Caco-2 cells, the positive control has a percentage of 30.29%; in the negative control, it is 98.96%.

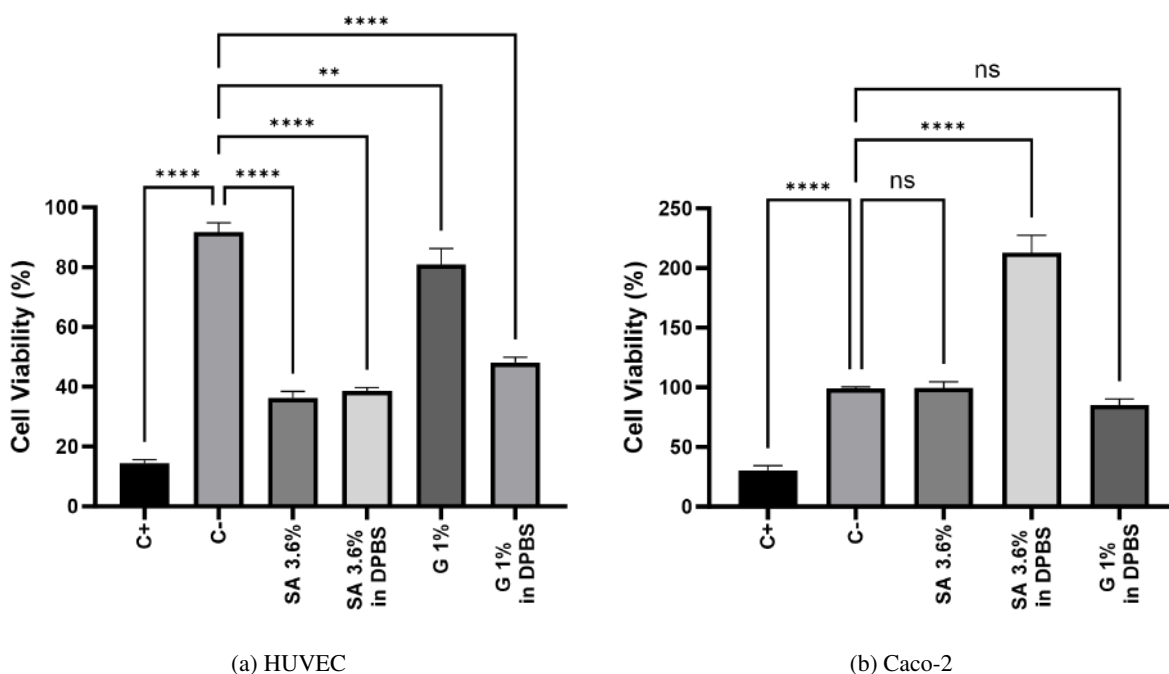


Figure 5.13: Cell viability of (a) HUVEC and (b) Caco-2 in alginate and gelatin using MTT assay. In the legend, "****" indicates $p < 0.0001$, "***" represents $p < 0.01$, and "ns" indicates non-significant.

Regarding Figure 5.13a, a) represents the viability values of the HUVEC cells seeded. In G 1%, the percentage was 80.97%, with a P value of 0.0025, indicating low toxicity. On the other hand, SA 3.6%, SA 3.6% in DPBS, and G 1% in DPBS indicated that the cells are not viable since the percentages obtained are between 36.27% and 48.12%. The viability of Caco-2 in SA 3.6% solved in DPBS showed statistically higher cell viability (212%), indicating a higher proliferation rate in this sample than controls. In SA 3.6%, G 1% in DPBS, values are below the percentage of the negative control (Figure 5.13b).

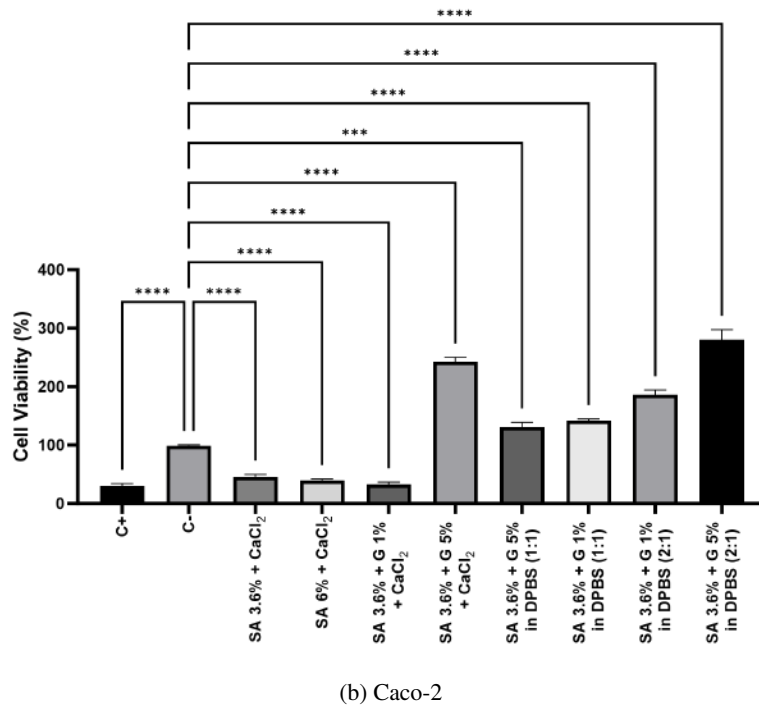
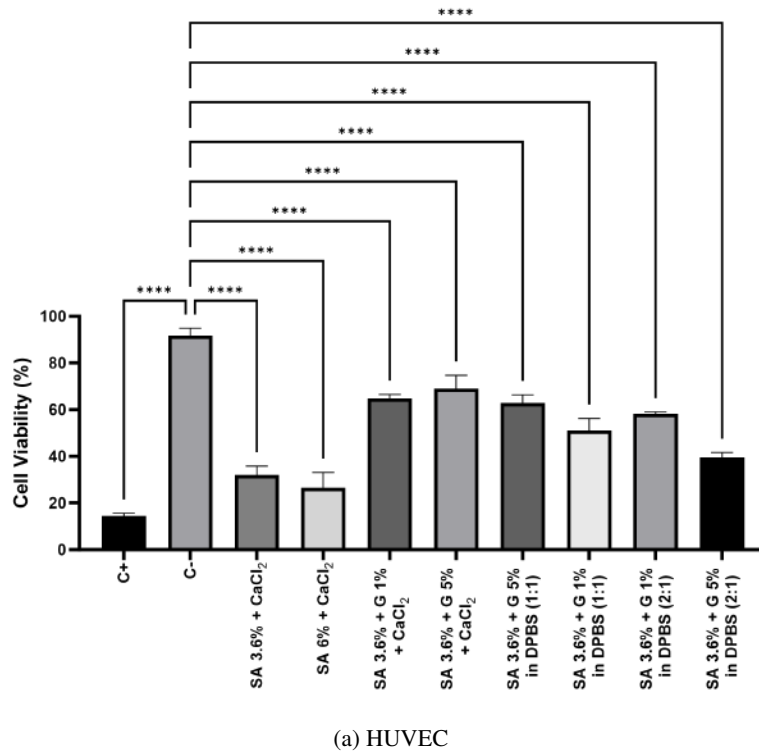


Figure 5.14: Cell viability of (a) HUVEC and (b) Caco-2 in SA and composites SA/G with $CaCl_2$ using MTT assay. In the legend, "****" indicates $p < 0.0001$, and "****" represents $p < 0.001$.

In figure 5.14a, the hydrogels composed of sodium alginate, gelatin and $CaCl_2$ show values above 60% compared with other materials where HUVEC were seeded. The viability percentage for SA 3.6% +G 1% + $CaCl_2$ was 64.91%, for SA 3.6% +G 5% + $CaCl_2$ was 68.92%, and for SA 3.6% +G 5% in DPBS was 62.84%. However, it is not possible to affirm that cells are completely viable in these materials. In the case of MTT for Caco-2, the materials that show viability above negative control are the mix of SA 3.6% +G 5% + $CaCl_2$ and SA 3.6% +G 5% solved in DPBS (Figure 5.14b).

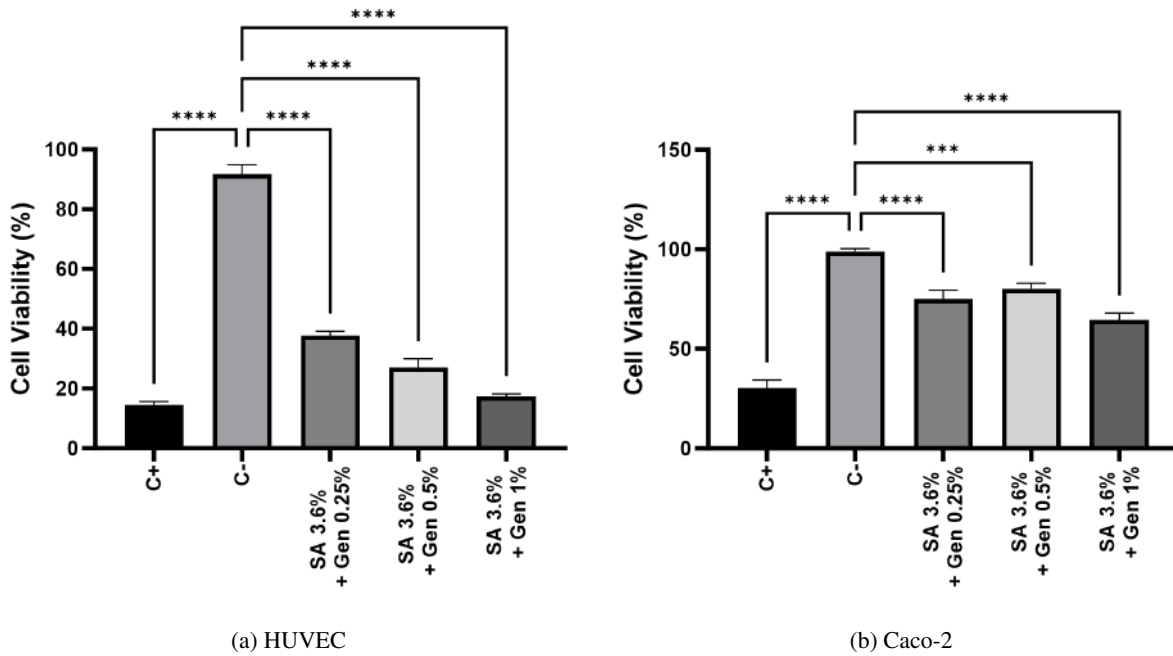


Figure 5.15: Cell viability of (a) HUVEC and (b) Caco-2 in sodium alginate with genipin using MTT assay. In the legend, "*****" indicates $p < 0.0001$, and "****" represents $p < 0.001$.

Figure 5.15a presents HUVEC cells' viability in SA crosslinked with genipin at different concentrations. It is possible to note that cells are not significantly viable in these materials. However, if the concentration of genipin is low (0.25%), the percentage of viability increases at 37.71%. For MTT of Caco-2, the cells show similar behavior, but the materials (SA 3.6% + Gen0.5%) show a viability of 80.15%, which does not have a significant difference with respect to genipin 0.25% (75.07%) (Figure 5.15b).

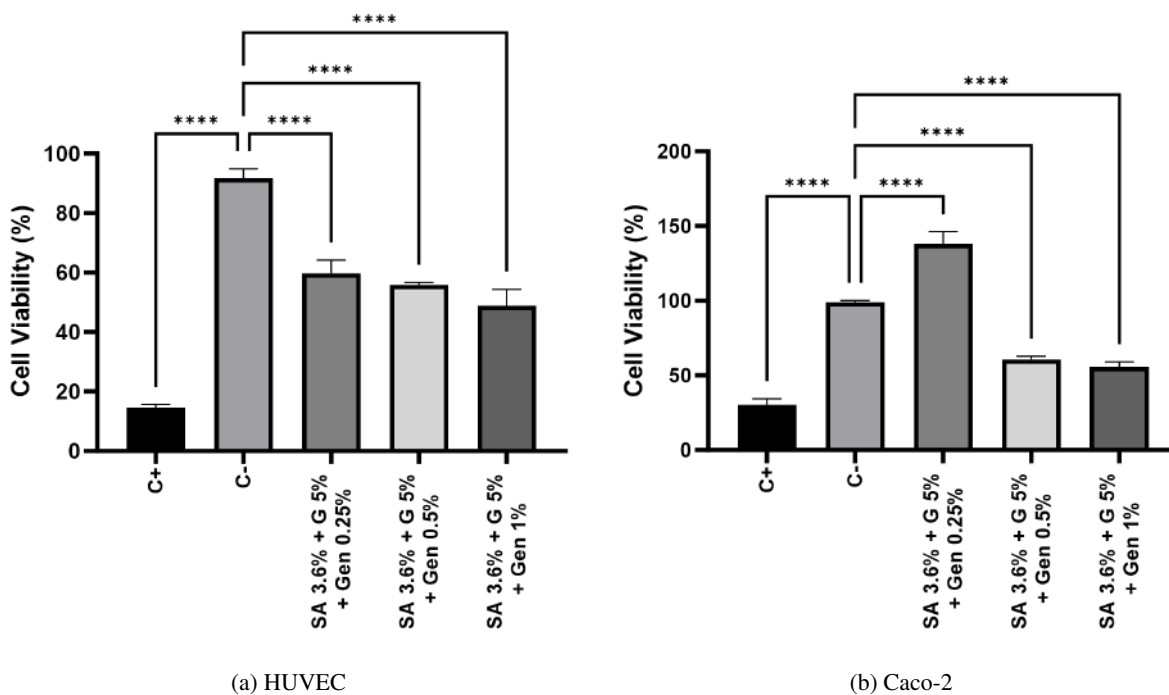


Figure 5.16: Cell viability of (a) HUVEC and (b) Caco-2 in the sodium alginate and gelatin with genipin using MTT assay. In the legend, "****" indicates $p < 0.0001$.

Figure 5.16a, the result of HUVEC cells' viability in SA and G crosslinked with genipin at different concentrations indicates that with a low concentration of genipin, the percentage of viability is 60% (Gen 0.25%). For MTT of Caco-2, the cells also show similar behavior with a percentage of 138.1%, above the negative control. However, the percentages of Gen 0.5% and 1% are between 55 to 60 % (Figure 5.16b).

5.4 Optical microscopy of cells lines

5.4.1 HUVEC cells

The optical microscopies were obtained after 12 hours of cell incubation with the materials. To analyze the growth, adhesion and confluence of HUVEC cells, the research article of Peng et al.⁹⁶ and Urbaczek et al.⁸¹ were used as a reference.

Figure 5.17 shows the micrography of HUVEC cells at $100\mu\text{m}$ and $20\mu\text{m}$. Figure 5.17b shows HUVEC cells that were incubated in a glove, a sterile material, in a culture medium. Cells could not grow and reach the morphology they have when growing in their culture medium, as shown in figure 5.17b, where the cells are confluent, and it is possible to see the spiral pattern.

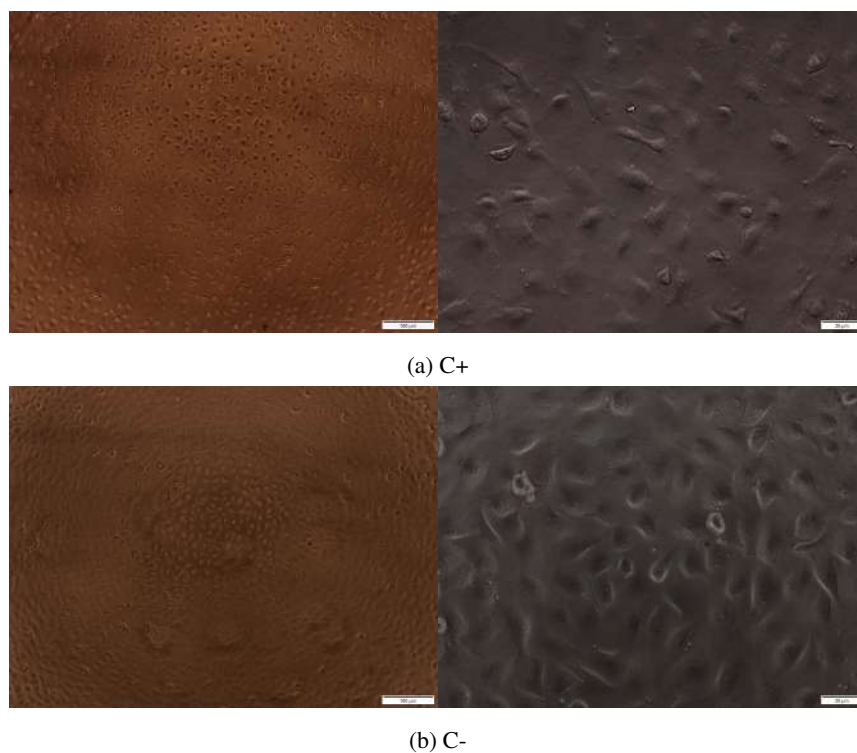


Figure 5.17: Optical microscopy of (a) positive control and (b) negative control of the HUVEC cell at different magnifications. Scale bar: $100\mu\text{m}$ (left) and $20\mu\text{m}$ (right).

Figure 5.18 shows the HUVEC cells in hydrogels of gelatin, alginate and genipin that have different concentrations. Figure 5.18c shows that the cells had no adhesion in materials because spherical shapes were observed, so cells present non-confluence. In Figure 5.18b, however, there was greater adhesion growth, and they reached the characteristic morphology in the cell. Cell proliferation could also be observed in figure 5.18a. However, there is a stretching of

the cells that indicates apoptosis. These observations are consistent with MTT trials.

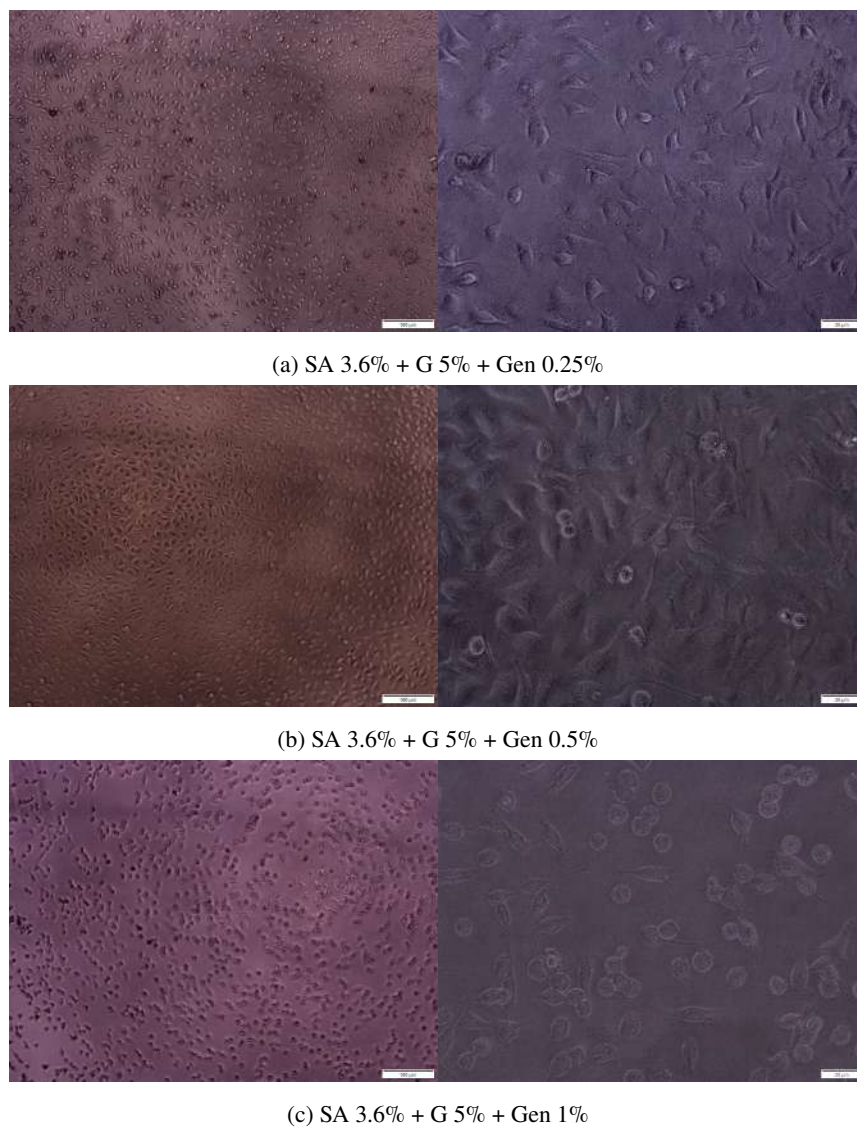
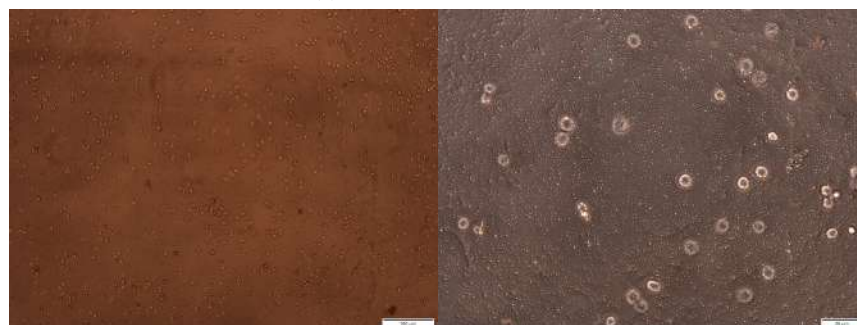


Figure 5.18: Optical microscopy of hydrogels composed by SA, G, and Gen in the HUVEC cell specified in (a), (b) and (c) at different magnifications. Scale bar: $100\mu\text{m}$ (left) and $20\mu\text{m}$ (right).

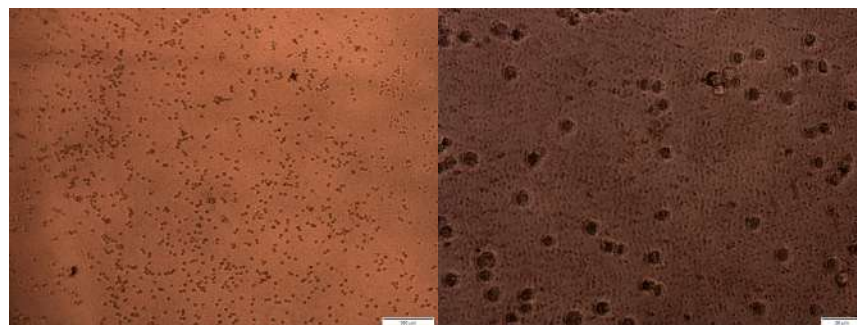
HUVEC cells in hydrogels of alginate and genipin are shown in Figure 5.19. In all samples, HUVEC conserves a spherical shape and non-confluence. However, the cellular adhesion on the materials can be noticed in Figure 5.19a and 5.19b.



(a) SA 3.6% + Gen 0.25%



(b) SA 3.6% + Gen 0.5%



(c) SA 3.6% + Gen 1%

Figure 5.19: Optical microscopy of hydrogels composed by SA and Gen in the HUVEC cell specified in (a), (b) and (c) in the HUVEC cell at different magnifications. Scale bar: $100\mu\text{m}$ (left) and $20\mu\text{m}$ (right).

In Figure 5.20, the cells seeded in alginate, regardless of the solvent used, show little growth, in addition to the elongation of the cells in their morphology, which, according to the literature, would indicate that there is apoptosis. However, in gelatin gels, there is greater cell growth. Specifically, this can be seen in Figure 5.20c corresponding to gelatin, where the characteristic morphology of HUVEC cells is shown.

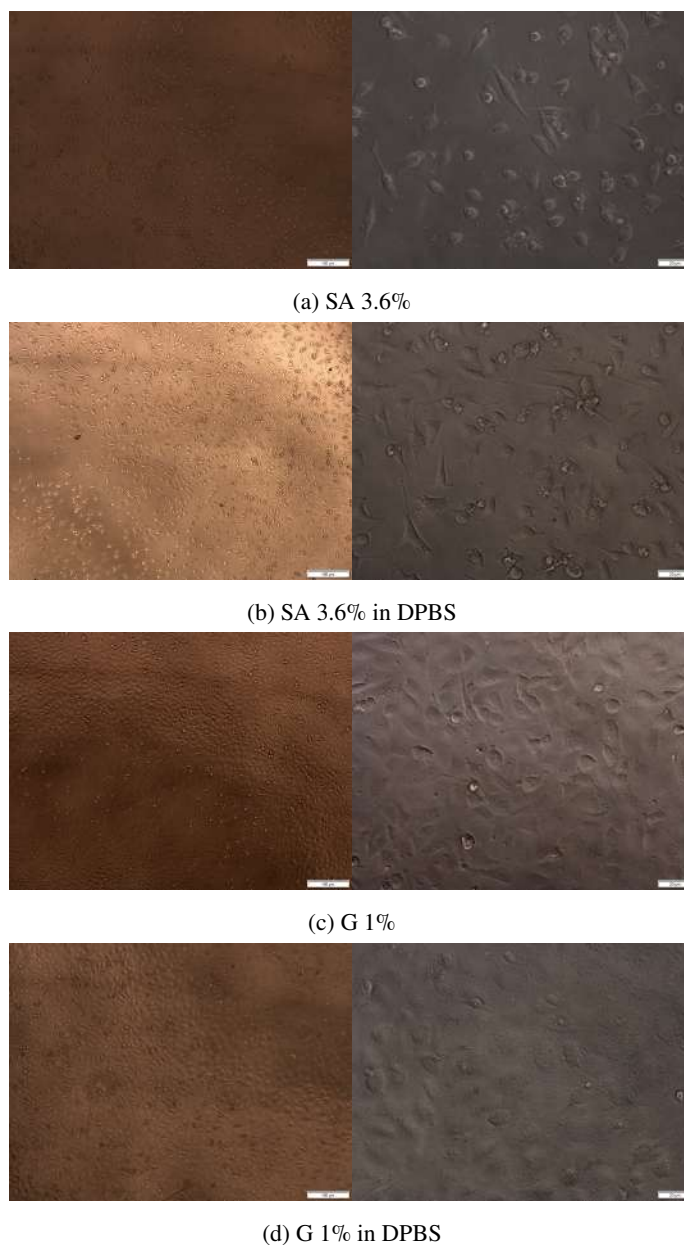
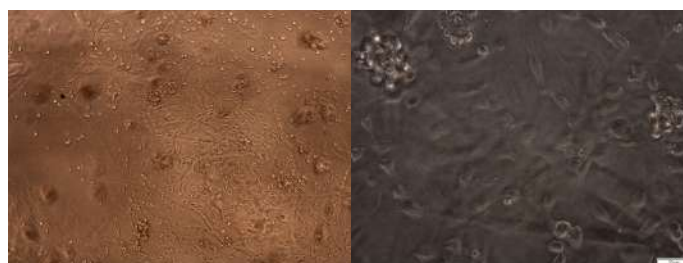


Figure 5.20: Optical microscopy of HUVEC cells in materials such as SA and G solved in distilled water and DPBS. Scale bar: 100 μ m (left) and 20 μ m (right).

The cells seeded on the alginate with $CaCl_2$ materials (Figure 5.21) did not adhere as much as on the alginate, gelatin and $CaCl_2$ materials. For example, there was greater proliferation in Figure 5.21c, and the cell morphology

is easily identified.



(a) SA 3.6% + $CaCl_2$



(b) SA 6% + $CaCl_2$



(c) SA 3.6% + G1% + $CaCl_2$



(d) SA 3.6% + G 5% + $CaCl_2$

Figure 5.21: Optical microscopy of hydrogels of SA and G crosslinking with $CaCl_2$ in HUVEC cells. Scale bar: $100\mu m$ (left) and $20\mu m$ (right).

Finally, Figure 5.22 shows that the cells in the materials dissolved in DPBS have greater growth in those that use a lower proportion of alginate. However, it does not reach confluence.



(a) SA 3.6% + G5% (1:1)



(b) SA 6% + G1% (1:1)



(c) SA 3.6% + G1% (2:1)



(d) SA 3.6% + G5% (2:1)

Figure 5.22: Optical microscopy of HUVEC cells on hydrogels of SA and G solved in DPBS. Scale bar: $100\mu\text{m}$ (left) and $20\mu\text{m}$ (right).

5.4.2 Caco-2 cells

Below, the microscopies obtained from the Caco-2 cell line are presented, and its growth is evaluated in the different materials prepared according to the morphology that this cell presents in the literature⁷⁷.

In the positive control (Figure 5.23a, where the cell has contact with a sterile material, it does not show growth but does show agglomeration of dead cells. On the other hand, in the positive control (Figure 5.23b), where the cells are maintained with the nutrients provided by the medium, we see cell adhesion and growth, so its morphology can be appreciated.

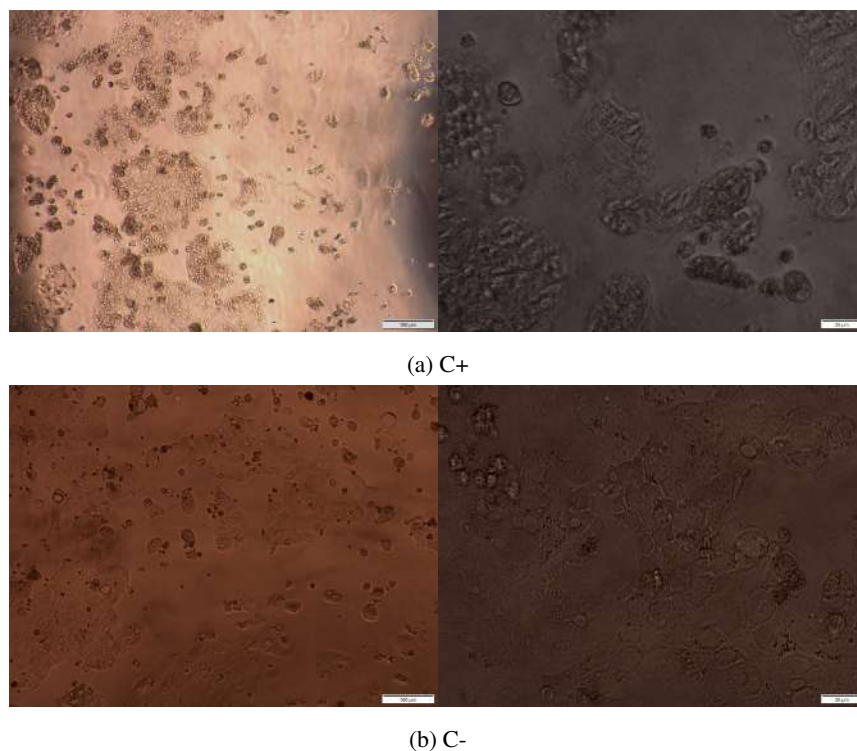
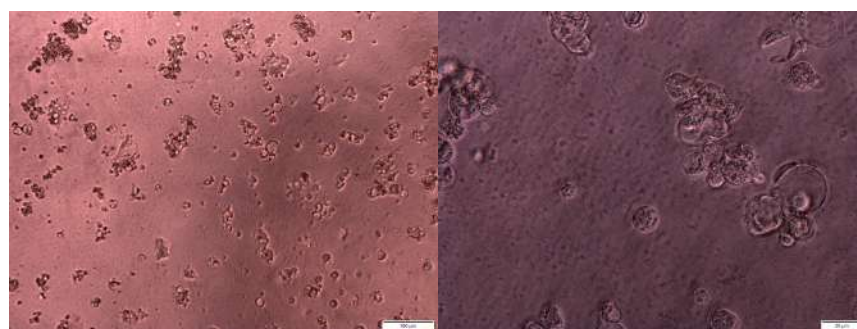
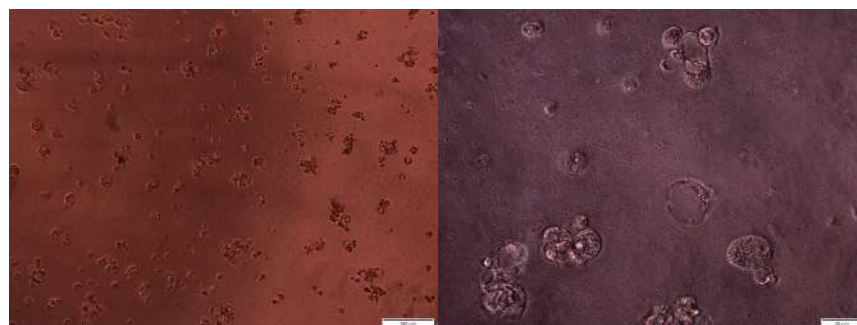


Figure 5.23: Optical microscopy of (a) positive control and (b) negative control of Caco-2 cell at different magnifications. Scale bar: 100 μm (left) and 20 μm (right).

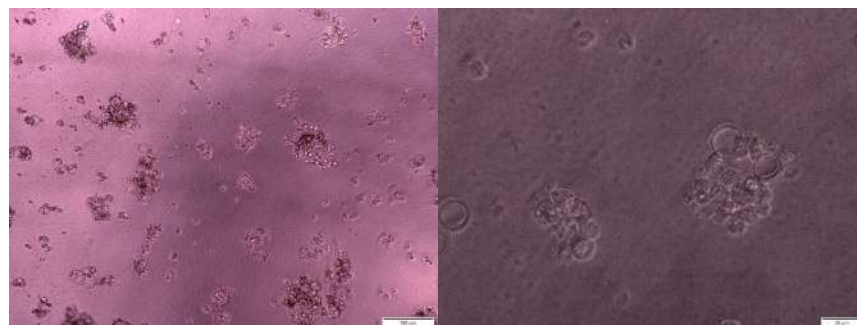
Figure 5.24 shows the Caco-2 cells in hydrogels of SA, G, and Gen. There is a confluence of Caco-2 cells, and it is possible to appreciate the rouns and small morphology. However, there is not a lot of adherence to the material.



(a) SA 3.6% + G 5% + Gen 0.25%



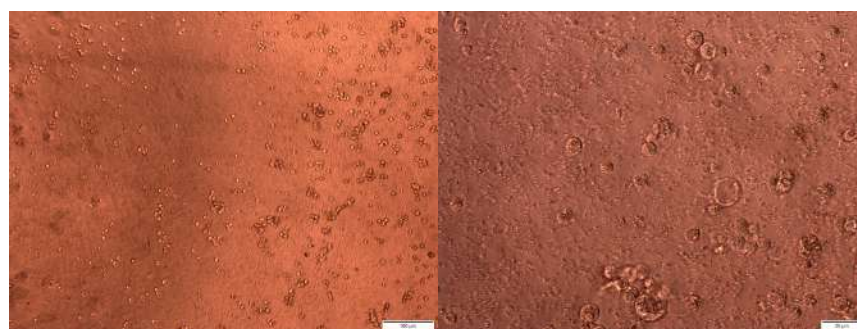
(b) SA 3.6% + G 5% + Gen 0.5%



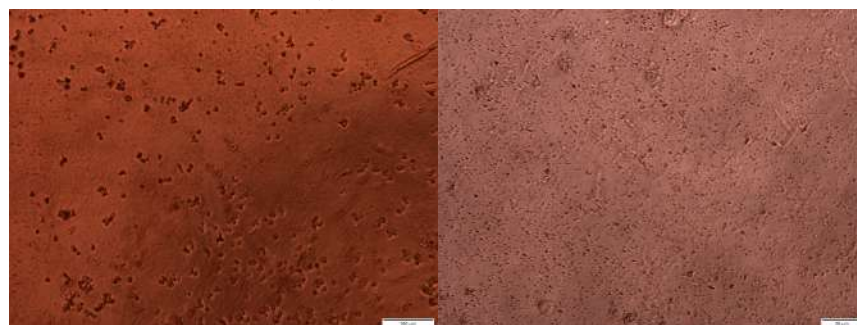
(c) SA 3.6% + G 5% + Gen 1%

Figure 5.24: Optical microscopy of hydrogels composed by SA, G, and Gen in the Caco-2 cells specified in (a), (b) and (c) at different magnifications. Scale bar: $100\mu\text{m}$ (left) and $20\mu\text{m}$ (right).

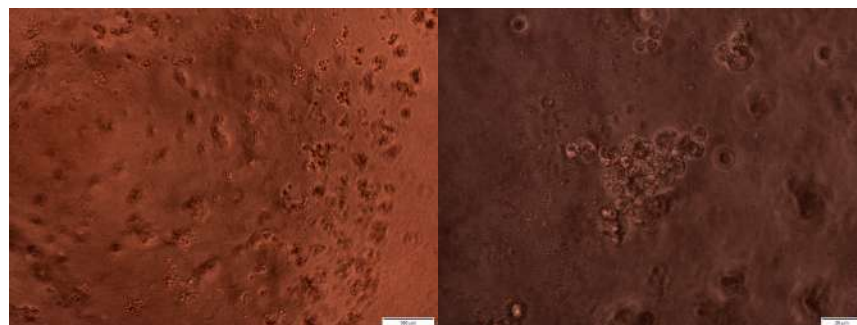
The cells maintained their round shape in the hydrogel composed of alginate and genipin (Figure 5.25). However, no adhesion or confluence could be observed, so the material does not allow the cell to grow.



(a) SA 3.6% + Gen 0.25%



(b) SA 3.6% + Gen 0.5%



(c) SA 3.6% + Gen 1%

Figure 5.25: Optical microscopy of hydrogels composed by SA and Gen in the HUVEC cell specified in (a), (b) and (c) in the Caco-2 cells at different magnifications. Scale bar: $100\mu\text{m}$ (left) and $20\mu\text{m}$ (right).

Figure 5.26 shows the microscopy results corresponding to the materials used to make the hydrogels. In sodium alginate, cells do not adhere but retain their round shape. The figure shows that the number of cells that can be observed is relatively low. Figure 5.26c showed morphological changes and indicated high confluence.

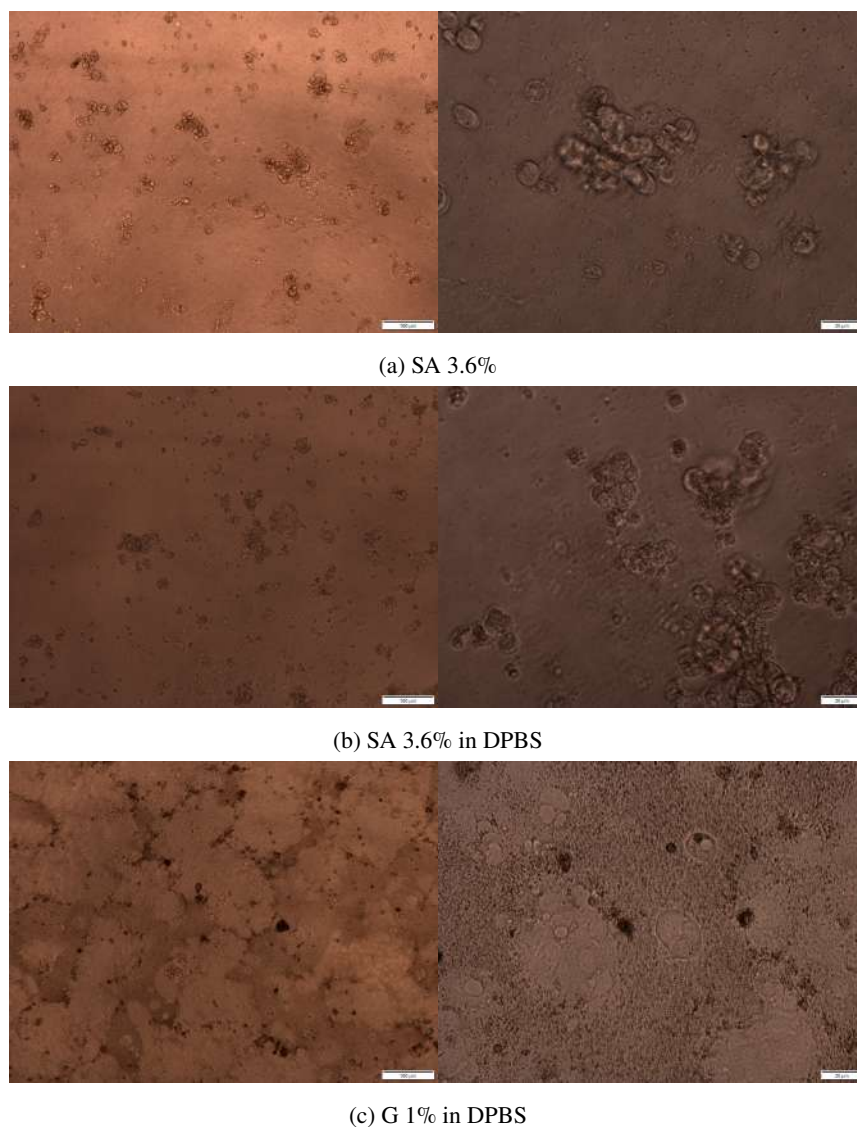


Figure 5.26: Optical microscopy of Caco-2 cells in materials such as SA and G solved in distilled water and DPBS. Scale bar: $100\mu\text{m}$ (left) and $20\mu\text{m}$ (right).

Figure 5.27 shows the cells on the hydrogels cross-linked with CaCl_2 . In Figure 5.27a, the cells do not adhere but have the characteristic round shape; no proliferation is observed. Figure 5.27b shows that the cell is confluent at a higher alginate concentration. On the other hand, hydrogels are composed of alginate gelatin, in which the cell does not have much proliferation when the gelatin concentration is low. However, in Figure 5.27d, apart from the cell showing confluence, it adheres to the material.

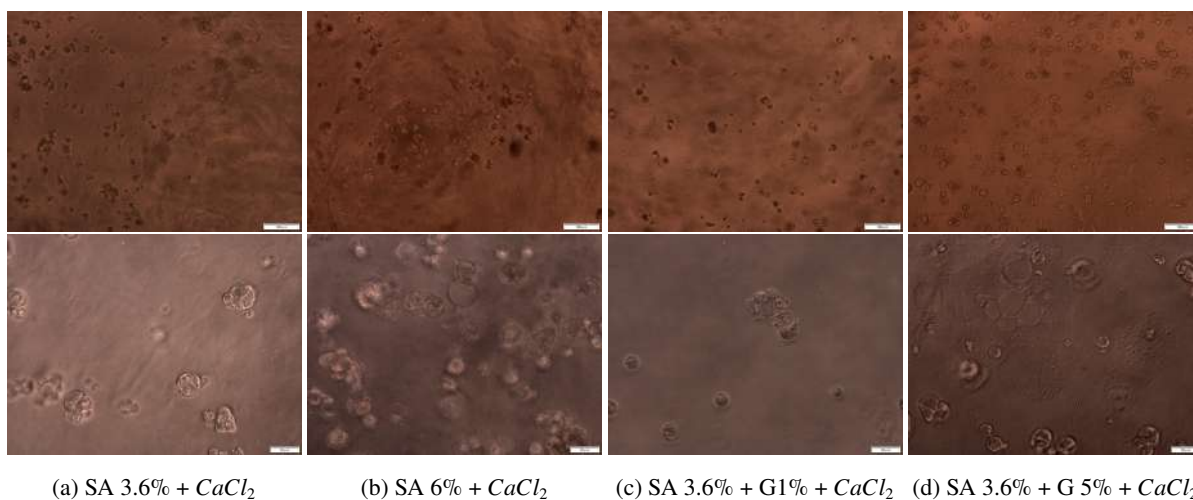


Figure 5.27: Optical microscopy of hydrogels of SA and G crosslinking with $CaCl_2$ in Caco-2 cells. Scale bar: $100\mu m$ (first row) and $20\mu m$ (second row).

Finally, hydrogels dissolved in DPBS can provide an environment where cells can develop if the gelatin concentration increases. In Figure 5.28a, the gelatin concentration is 5%, and the cells are not confluent but reaching their morphology and adhering to the material. In the materials in Figures 5.28b and 5.28c, adhesion cannot be observed; however, the characteristic morphology of the cells is possible to see. In Figure 5.28d, however, we see that the cell manages to adhere, but there is little proliferation.

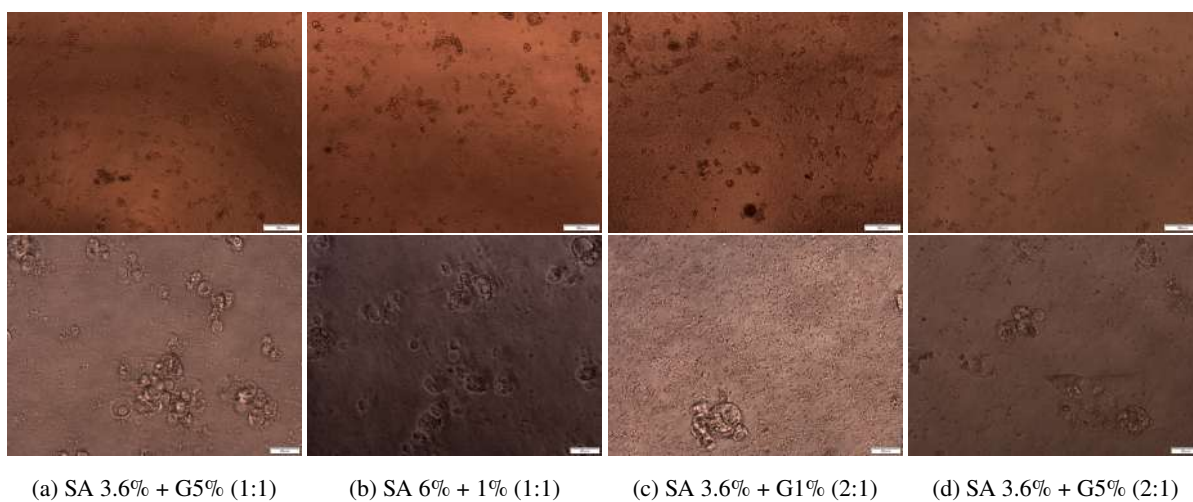


Figure 5.28: Optical microscopy Caco-2 cells on hydrogels of SA and G solved in DPBS. Scale bar: $100\mu m$ (first row) and $20\mu m$ (second row).

This section analyzed the hydrogels of alginate and gelatin prepared in the present study with the concentrations that provide the best mechanical characteristics. First, through FT-IR analysis, it was possible to visualize the characteristic bands of all the materials used, such as sodium alginate that is characterized by having $-\text{COO}-$ bonds, gelatin that has amides, genipin with its aldehyde group, DPBS with phosphate groups, and CaCl_2 .

Analyzing all hydrogels' crosslinking and molecular interactions is also possible according to their composition. So, FTIRs show band shifting, such as in alginate with CaCl_2 , which indicates Ca^{2+} ions interact with the alginate molecules. In the case of the mixture of alginate with gelatin, it was confirmed that there was a molecular interaction because the Amide I band of the gelatin was coupled to the band of strong absorption of the SA. Similarly, in the interaction between alginate and genipin, a change in the intensity and position of the vibrations associated with the carboxylate groups can be observed. If genipin interacted with gelatin, it was possible to see the conservation of the peaks corresponding to the amides, which is where the aldehyde group of genipin is attached. Moreover, in the preparation of composites with genipin, it was possible to observe a change of color to blue, which is characteristic when the crosslinking is done^{53,89,94,97}.

The morphology was evaluated using the SEM, and according to the literature^{66,95,98}, it is known that a porous microstructure is essential for biocompatibility and for cells to be housed. Moreover, porosity facilitates connectivity, allowing nutrients and oxygen into the inner regions and eliminating cellular waste²¹. According to the analysis, all samples had porosity, but the pore size varied greatly. The sample that shows a stable relationship in this case is the one that corresponds to the composition of SA with G cross-linked with CaCl_2 .

Regarding cell viability assays, by exposing the HUVEC cells to the different materials and hydrogels prepared, we can corroborate that gelatin provides an environment where the cell can develop; the percentage viability of HUVEC cells presented was 80.97%. The hydrogels presented viability above 60%; they were composed of SA 3.6% G 5% cross-linked with genipin or CaCl_2 . Based on the results, it can also be stated that while the genipin concentration is lower, the cell survival rate is higher since better results were obtained when the concentration was 0.25%.

When the same study was carried out, but with the Caco-2 cell line, favorable results were obtained in alginate dissolved in PBS, in hydrogels composed of 3.6% alginate, 5% gelatin cross-linked with either genipin or CaCl_2 . Furthermore, these cells showed a survival rate in the hydrogels dissolved in PBS. These results are consistent when analyzing the images obtained by optical microscopy, where it can be observed that the cells adhere to the material and reach confluence. It is the case of HUVEC, which is shown growing in a spiral pattern characteristic of this cell line, and in the case of Caco-2, where it is shown to have a spheroid shape, as its morphology is described in the literature^{77,81}.

Considering the morphological characteristics and feasibility studies, the ink that could be used to make the fabric is the one that is composed of alginate, gelatin, and CaCl_2 . However, the compound cross-linked with genipin shows good results. Therefore, if an optimal concentration is standardized, this could also be a promising composition as it is a compound of natural origin for both cell lines.

Chapter 6

Conclusions & Outlook

This work reports the synthesis and characterization of alginate/gelatin hydrogels for their potential application as bioinks for 3D human tissue models. FT-IR spectroscopy allows seeing the characteristics bands produced by the vibration of compounds and the band shifting when the crosslinking of hydrogels takes place. Scanning electron micrographs show the structural properties and the porosity for MTT and cell viability. The obtained results reveal that the hydrogel that presents the greatest biocompatibility with these cell lines is the one composed of SA 3.6%, G5%, and $CaCl_2$. However, it was possible to analyze that genipin is also an excellent method of cross-linking. To obtain greater viability with this agent, another study is intended to be carried out where it has lower concentrations without the polymers losing stability.

As future research, to ensure that these tissue models reach their final application, whether, in vitro testing, disease modeling or in vivo implantation, this stage of bioink selection will continue, with more studies being carried out to know the physical and mechanical properties of the materials through printability tests, rheological analyzes and swelling and degradation tests. To be used as a tumor model or in tissue engineering within biological characterization, it is also relevant to perform cytotoxicity and cell proliferation analyses to better understand the cellular response of the materials and determine if there are toxic effects.

Bibliography

- [1] Cadamuro, F.; Nicotra, F.; Russo, L. 3D printed tissue models: From hydrogels to biomedical applications. *Journal of Controlled Release* **2023**, *354*, 726–745.
- [2] Wong, C. H.; Siah, K. W.; Lo, A. W. Estimation of clinical trial success rates and related parameters. *Biostatistics* **2019**, *20*, 273–286.
- [3] Seyhan, A. A. Lost in translation: the valley of death across preclinical and clinical divide—identification of problems and overcoming obstacles. *Translational Medicine Communications* **2019**, *4*, 1–19.
- [4] Sbirkov, Y.; Molander, D.; Milet, C.; Bodurov, I.; Atanasov, B.; Penkov, R.; Belev, N.; Forraz, N.; McGuckin, C.; Sarafian, V. A colorectal cancer 3D bioprinting workflow as a platform for disease modeling and chemotherapeutic screening. *Frontiers in Bioengineering and Biotechnology* **2021**, 910.
- [5] Sung, H.; Ferlay, J.; Siegel, R. L.; Laversanne, M.; Soerjomataram, I.; Jemal, A.; Bray, F. Global cancer statistics 2020: GLOBOCAN estimates of incidence and mortality worldwide for 36 cancers in 185 countries. *CA: a cancer journal for clinicians* **2021**, *71*, 209–249.
- [6] Fang, W.; Yang, M.; Wang, L.; Li, W.; Liu, M.; Jin, Y.; Wang, Y.; Yang, R.; Wang, Y.; Zhang, K.; Fu, Q. Hydrogels for 3D bioprinting in tissue engineering and regenerative medicine: Current progress and challenges. *International Journal of Bioprinting* **2023**, *9*.
- [7] Shams, E.; Barzad, M. S.; Mohamadnia, S.; Tavakoli, O.; Mehrdadfar, A. A review on alginate-based bioinks, combination with other natural biomaterials and characteristics. *Journal of Biomaterials Applications* **2022**, *37*, 355–372.
- [8] Zhuang, X.; Deng, G.; Wu, X.; Xie, J.; Li, D.; Peng, S.; Tang, D.; Zhou, G. Recent advances of three-dimensional bioprinting technology in hepato-pancreato-biliary cancer models. *Frontiers in Oncology* **2023**, *13*, 1143600.
- [9] Parodi, I.; Di Lisa, D.; Pastorino, L.; Scaglione, S.; Fato, M. M. 3D Bioprinting as a Powerful Technique for Recreating the Tumor Microenvironment. *Gels* **2023**, *9*, 482.

- [10] Zhao, W.; Xu, T. Preliminary engineering for in situ in vivo bioprinting: a novel micro bioprinting platform for in situ in vivo bioprinting at a gastric wound site. *Biofabrication* **2020**, *12*, 045020.
- [11] Chaji, S.; Al-Saleh, J.; Gomillion, C. T. Bioprinted three-dimensional cell-laden hydrogels to evaluate adipocyte-breast cancer cell interactions. *Gels* **2020**, *6*, 10.
- [12] Hiller, T.; Berg, J.; Elomaa, L.; Röhrs, V.; Ullah, I.; Schaar, K.; Dietrich, A.-C.; Al-Zeer, M. A.; Kurtz, A.; Hocke, A. C.; Hippenstiel, S.; Fechner, H.; Weinhart, M.; Kurreck, J. Generation of a 3D Liver Model Comprising Human Extracellular Matrix in an Alginate/Gelatin-Based Bioink by Extrusion Bioprinting for Infection and Transduction Studies. *International Journal of Molecular Sciences* **2018**, *19*.
- [13] Ketabat, F.; Maris, T.; Duan, X.; Yazdanpanah, Z.; Kelly, M. E.; Badea, I.; Chen, X. Optimization of 3D printing and in vitro characterization of alginate/gelatin lattice and angular scaffolds for potential cardiac tissue engineering. *Frontiers in Bioengineering and Biotechnology* **2023**, *11*, 1161804.
- [14] Mondal, A.; Gebeyehu, A.; Miranda, M.; Bahadur, D.; Patel, N.; Ramakrishnan, S.; Rishi, A. K.; Singh, M. Characterization and printability of Sodium alginate-Gelatin hydrogel for bioprinting NSCLC co-culture. *Scientific reports* **2019**, *9*, 19914.
- [15] Rosińska, K.; Bartniak, M.; Wierzbicka, A.; Sobczyk-Guzenda, A.; Bociaga, D. Solvent types used for the preparation of hydrogels determine their mechanical properties and influence cell viability through gelatine and calcium ions release. *Journal of Biomedical Materials Research Part B: Applied Biomaterials* **2023**, *111*, 314–330.
- [16] Saeidnia, S.; Manayi, A.; Abdollahi, M. From in vitro experiments to in vivo and clinical studies; pros and cons. *Current drug discovery technologies* **2015**, *12*, 218–224.
- [17] Ng, W. L.; Win Naing, M.; Suntornnond, R.; Vijayavenkataraman, S. Fabrication of in-vitro 3D human tissue models—From cell processing to advanced manufacturing. *Frontiers in Bioengineering and Biotechnology* **2022**, *10*, 1035601.
- [18] Francois, P.; Mario, B.; CM, B. H.; Andreas, C.; Gordon, D.; Philip, H.; Tomas, M.; Teija, O.; Adrian, R.; Thomas, S.-H. The evolving role of investigative toxicology in the pharmaceutical industry. *Nature reviews drug discovery* **2023**, *22*, 317–335.
- [19] Tavassoli, H.; Alhosseini, S. N.; Tay, A.; Chan, P. P.; Oh, S. K. W.; Warkiani, M. E. Large-scale production of stem cells utilizing microcarriers: a biomaterials engineering perspective from academic research to commercialized products. *Biomaterials* **2018**, *181*, 333–346.
- [20] Shyam, R.; Reddy, L. V. K.; Palaniappan, A. Fabrication and Characterization Techniques of In Vitro 3D Tissue Models. *International Journal of Molecular Sciences* **2023**, *24*, 1912.

- [21] Raees, S.; Ullah, F.; Javed, F.; Akil, H. M.; Jadoon Khan, M.; Safdar, M.; Din, I. U.; Alotaibi, M. A.; Alharthi, A. I.; Bakht, M. A.; Ahmad, A.; Nassar, A. A. Classification, processing, and applications of bioink and 3D bioprinting: A detailed review. *International Journal of Biological Macromolecules* **2023**, *232*, 123476.
- [22] Li, J.; Chen, M.; Fan, X.; Zhou, H. Recent advances in bioprinting techniques: approaches, applications and future prospects. *Journal of translational medicine* **2016**, *14*, 1–15.
- [23] Tamay, D. G.; Dursun Usal, T.; Alagoz, A. S.; Yucel, D.; Hasirci, N.; Hasirci, V. 3D and 4D printing of polymers for tissue engineering applications. *Frontiers in bioengineering and biotechnology* **2019**, *7*, 164.
- [24] Ozbolat, I. T.; Hospodiuk, M. Current advances and future perspectives in extrusion-based bioprinting. *Biomaterials* **2016**, *76*, 321–343.
- [25] Pavan Kalyan, B.; Kumar, L. 3D printing: applications in tissue engineering, medical devices, and drug delivery. *Aaps Pharmscitech* **2022**, *23*, 92.
- [26] Derakhshanfar, S.; Mbeleck, R.; Xu, K.; Zhang, X.; Zhong, W.; Xing, M. 3D bioprinting for biomedical devices and tissue engineering: A review of recent trends and advances. *Bioactive materials* **2018**, *3*, 144–156.
- [27] Kulkarni, R.; Pandya, A. 3D bioprinting: overview and recent developments. *Design, Principle and Application of Self-Assembled Nanobiomaterials in Biology and Medicine* **2022**, 149–171.
- [28] Groll, J.; Burdick, J. A.; Cho, D.-W.; Derby, B.; Gelinsky, M.; Heilshorn, S. C.; Jüngst, T.; Malda, J.; Mironov, V. A.; Nakayama, K.; Ovsianikov, A.; Sun, W.; Takeuchi, S.; Yoo, J. J.; Woodfield, T. B. F. A definition of bioinks and their distinction from biomaterial inks. *Biofabrication* **2018**, *11*, 013001.
- [29] Montero, F. E.; Rezende, R. A.; Da Silva, J. V.; Sabino, M. A. Development of a smart bioink for bioprinting applications. *Frontiers in Mechanical Engineering* **2019**, *5*, 56.
- [30] Hospodiuk, M.; Dey, M.; Sosnoski, D.; Ozbolat, I. T. The bioink: A comprehensive review on bioprintable materials. *Biotechnology advances* **2017**, *35*, 217–239.
- [31] Chen, X.; Anvari-Yazdi, A. F.; Duan, X.; Zimmerling, A.; Gharraei, R.; Sharma, N.; Sweilem, S.; Ning, L. Biomaterials/bioinks and extrusion bioprinting. *Bioactive Materials* **2023**, *28*, 511–536.
- [32] Axpe, E.; Oyen, M. L. Applications of alginate-based bioinks in 3D bioprinting. *International journal of molecular sciences* **2016**, *17*, 1976.
- [33] Das, S.; Basu, B. An overview of hydrogel-based bioinks for 3D bioprinting of soft tissues. *Journal of the Indian Institute of Science* **2019**, *99*, 405–428.
- [34] Kaliaraj, G. S.; Shanmugam, D. K.; Dasan, A.; Mosas, K. K. A. Hydrogels—A Promising Materials for 3D Printing Technology. *Gels* **2023**, *9*, 260.

- [35] Fatimi, A.; Okoro, O. V.; Podstawczyk, D.; Siminska-Stanny, J.; Shavandi, A. Natural hydrogel-based bio-inks for 3D bioprinting in tissue engineering: A review. *Gels* **2022**, *8*, 179.
- [36] Lima, T. d. P.; Canelas, C. A. d. A.; Concha, V. O.; Costa, F. A. d.; Passos, M. F. 3D Bioprinting Technology and Hydrogels Used in the Process. *Journal of Functional Biomaterials* **2022**, *13*, 214.
- [37] Tajik, S.; Garcia, C. N.; Gillooley, S.; Tayebi, L. 3D Printing of Hybrid-Hydrogel Materials for Tissue Engineering: A Critical Review. *Regenerative Engineering and Translational Medicine* **2023**, *9*, 29–41.
- [38] Hennink, W. E.; van Nostrum, C. F. Novel crosslinking methods to design hydrogels. *Advanced drug delivery reviews* **2012**, *64*, 223–236.
- [39] Gao, T.; Gillispie, G. J.; Copus, J. S.; Pr, A. K.; Seol, Y.-J.; Atala, A.; Yoo, J. J.; Lee, S. J. Optimization of gelatin–alginate composite bioink printability using rheological parameters: A systematic approach. *Biofabrication* **2018**, *10*, 034106.
- [40] Li, N.; Guo, R.; Zhang, Z. J. Bioink formulations for bone tissue regeneration. *Frontiers in Bioengineering and Biotechnology* **2021**, *9*, 630488.
- [41] Krishnakumar, G. S.; Sampath, S.; Muthusamy, S.; John, M. A. Importance of crosslinking strategies in designing smart biomaterials for bone tissue engineering: A systematic review. *Materials Science and Engineering: C* **2019**, *96*, 941–954.
- [42] Beata Łabowska, M.; Michalak, I.; Detyna, J. Methods of extraction, physicochemical properties of alginates and their applications in biomedical field—a review. *Open Chemistry* **2019**, *17*, 738–762.
- [43] Loureiro dos Santos, L. *Natural Polymeric Biomaterials: Processing and Properties*; Elsevier, 2017.
- [44] Bhatia, A. K.; Dewangan, S.; Vaidya, N. *Computational Modelling and Simulations for Designing of Corrosion Inhibitors*; Elsevier, 2023; pp 435–460.
- [45] Faramarzi, N.; Yazdi, I. K.; Nabavinia, M.; Gemma, A.; Fanelli, A.; Caizzone, A.; Ptaszek, L. M.; Sinha, I.; Khademhosseini, A.; Ruskin, J. N.; Tamayol, A. Patient-Specific Bioinks for 3D Bioprinting of Tissue Engineering Scaffolds. *Advanced Healthcare Materials* **2018**, *7*, 1701347.
- [46] Zhang, Y.; Yu, W.; Lv, G.; Zhu, J.; Wang, W.; Ma, X.; Liu, X. The artificial organ: Cell encapsulation. **2011**,
- [47] Deshmukh, K.; Ahamed, M. B.; Deshmukh, R.; Pasha, S. K.; Bhagat, P.; Chidambaram, K. *Biopolymer composites in electronics*; Elsevier, 2017; pp 27–128.
- [48] Wang, X.; Ao, Q.; Tian, X.; Fan, J.; Tong, H.; Hou, W.; Bai, S. Gelatin-based hydrogels for organ 3D bioprinting. *Polymers* **2017**, *9*, 401.

- [49] Ashammakhi, N.; Ahadian, S.; Xu, C.; Montazerian, H.; Ko, H.; Nasiri, R.; Barros, N.; Khademhosseini, A. Bioinks and bioprinting technologies to make heterogeneous and biomimetic tissue constructs. *Materials Today Bio* **2019**, *1*, 100008.
- [50] Chung, J. H.; Naficy, S.; Yue, Z.; Kapsa, R.; Quigley, A.; Moulton, S. E.; Wallace, G. G. Bio-ink properties and printability for extrusion printing living cells. *Biomaterials Science* **2013**, *1*, 763–773.
- [51] Bociaga, D.; Bartniak, M.; Grabarczyk, J.; Przybyszewska, K. Sodium alginate/gelatine hydrogels for direct bioprinting—The effect of composition selection and applied solvents on the bioink properties. *Materials* **2019**, *12*, 2669.
- [52] Jia, J.; Richards, D. J.; Pollard, S.; Tan, Y.; Rodriguez, J.; Visconti, R. P.; Trusk, T. C.; Yost, M. J.; Yao, H.; Markwald, R. R.; Mei, Y. Engineering alginate as bioink for bioprinting. *Acta biomaterialia* **2014**, *10*, 4323–31.
- [53] Utami Nike, D.; Md Fadilah, N. I.; Sallehuddin, N.; Nor Azlan, A. Y. H.; Imran, F. H.; Maarof, M.; Fauzi, M. B. Genipin-crosslinking effects on biomatrix development for Cutaneous wound healing: a concise review. *Frontiers in Bioengineering and Biotechnology* **2022**, *10*, 865014.
- [54] Harris, R.; Lecumberri, E.; Heras, A. Chitosan-genipin microspheres for the controlled release of drugs: clarithromycin, tramadol and heparin. *Marine drugs* **2010**, *8*, 1750–1762.
- [55] Tacias-Pascacio, V. G.; García-Parra, E.; Vela-Gutiérrez, G.; Virgen-Ortiz, J. J.; Berenguer-Murcia, Á.; Alcántara, A. R.; Fernandez-Lafuente, R. Genipin as an emergent tool in the design of biocatalysts: mechanism of reaction and applications. *Catalysts* **2019**, *9*, 1035.
- [56] Bellefeuille, M.; Peters, D.; Nolin, M.; Slusarewicz, P.; Telgenhoff, D. Examination of toxicity and collagen linearity after the administration of the protein cross-linker genipin in equine tendon and dermis: a pilot study. *Australian Veterinary Journal* **2017**, *95*, 167–173.
- [57] Wang, Z.; Liu, H.; Luo, W.; Cai, T.; Li, Z.; Liu, Y.; Gao, W.; Wan, Q.; Wang, X.; Wang, J.; Wang, Y.; Yang, X. Regeneration of skeletal system with genipin crosslinked biomaterials. *Journal of Tissue Engineering* **2020**, *11*.
- [58] Erdagi, S. I.; Ngwabebhoh, F. A.; Yildiz, U. Genipin crosslinked gelatin-diosgenin-nanocellulose hydrogels for potential wound dressing and healing applications. *International journal of biological macromolecules* **2020**, *149*, 651–663.
- [59] Berthomieu, C.; Hienerwadel, R. Fourier transform infrared (FTIR) spectroscopy. *Photosynthesis research* **2009**, *101*, 157–170.
- [60] Nicolet, T.; All, C. Introduction to fourier transform infrared spectrometry. *Thermo Nicolet Corporation* **2001**,

- [61] Mohamed, M. A.; Jaafar, J.; Ismail, A.; Othman, M.; Rahman, M. *Membrane characterization*; Elsevier, 2017; pp 3–29.
- [62] Patrizi, B.; Siciliani de Cumis, M.; Viciani, S.; D'Amato, F. Dioxin and related compound detection: Perspectives for optical monitoring. *International Journal of Molecular Sciences* **2019**, *20*, 2671.
- [63] Inkson, B. J. *Materials characterization using nondestructive evaluation (NDE) methods*; Elsevier, 2016; pp 17–43.
- [64] Kannan, M. Scanning electron microscopy: Principle, components and applications. *A textbook on fundamentals and applications of nanotechnology* **2018**, 81–92.
- [65] Schmitt, R. In *CIRP Encyclopedia of Production Engineering*; Laperrière, L., Reinhart, G., Eds.; Springer Berlin Heidelberg: Berlin, Heidelberg, 2014; pp 1085–1089.
- [66] Kaberova, Z.; Karpushkin, E.; Nevoralová, M.; Vetrík, M.; Šlouf, M.; Dušková-Smrčková, M. Microscopic structure of swollen hydrogels by scanning electron and light microscopies: Artifacts and reality. *Polymers* **2020**, *12*, 578.
- [67] Piccinini, F.; Tesei, A.; Arienti, C.; Bevilacqua, A. Cell counting and viability assessment of 2D and 3D cell cultures: expected reliability of the trypan blue assay. *Biological procedures online* **2017**, *19*, 1–12.
- [68] Strober, W. Trypan blue exclusion test of cell viability. *Current protocols in immunology* **1997**, *21*, A–3B.
- [69] Kamiloglu, S.; Sari, G.; Ozdal, T.; Capanoglu, E. Guidelines for cell viability assays. *Food Frontiers* **2020**, *1*, 332–349.
- [70] Kumar, P.; Nagarajan, A.; Uchil, P. D. Analysis of cell viability by the MTT assay. *Cold spring harbor protocols* **2018**, *2018*.
- [71] Sylvester, P. W. Optimization of the tetrazolium dye (MTT) colorimetric assay for cellular growth and viability. *Drug Design and Discovery: Methods and Protocols* **2011**, 157–168.
- [72] Mosmann, T. Rapid colorimetric assay for cellular growth and survival: application to proliferation and cytotoxicity assays. *Journal of immunological methods* **1983**, *65*, 55–63.
- [73] Präbst, K.; Engelhardt, H.; Ringgeler, S.; Hübner, H. Basic colorimetric proliferation assays: MTT, WST, and resazurin. *Cell viability assays: methods and protocols* **2017**, 1–17.
- [74] Lea, T. Caco-2 cell line. *The Impact of Food Bioactives on Health: in vitro and ex vivo models* **2015**, 103–111.
- [75] Macedo, M. H.; Martinez, E.; Barrias, C. C.; Sarmiento, B. Development of an improved 3D in vitro intestinal model to perform permeability studies of paracellular compounds. *Frontiers in bioengineering and biotechnology* **2020**, 1076.

- [76] Natoli, M.; Leoni, B. D.; D'Agnano, I.; Zucco, F.; Felsani, A. Good Caco-2 cell culture practices. *Toxicology in vitro* **2012**, *26*, 1243–1246.
- [77] Gheytaichi, E.; Naseri, M.; Karimi-Busheri, F.; Atyabi, F.; Mirsharif, E. S.; Bozorgmehr, M.; Ghods, R.; Madjd, Z. Morphological and molecular characteristics of spheroid formation in HT-29 and Caco-2 colorectal cancer cell lines. *Cancer cell international* **2021**, *21*, 1–16.
- [78] Medina-Leyte, D. J.; Domínguez-Pérez, M.; Mercado, I.; Villarreal-Molina, M. T.; Jacobo-Albavera, L. Use of human umbilical vein endothelial cells (HUVEC) as a model to study cardiovascular disease: A review. *Applied Sciences* **2020**, *10*, 938.
- [79] Marin, V.; Kaplanski, G.; Gres, S.; Farnarier, C.; Bongrand, P. Endothelial cell culture: protocol to obtain and cultivate human umbilical endothelial cells. *Journal of immunological methods* **2001**, *254*, 183–190.
- [80] Jaffe, E. A.; Nachman, R. L.; Becker, C. G.; Minick, C. R. Culture of human endothelial cells derived from umbilical veins. Identification by morphologic and immunologic criteria. *The Journal of clinical investigation* **1973**, *52* 11, 2745–56.
- [81] Urbaczek, A. C.; Leão, P. A. G. C.; Souza, F. Z. R. d.; Afonso, A.; Vieira Alberice, J.; Cappelini, L. T. D.; Carlos, I. Z.; Carrilho, E. Endothelial cell culture under perfusion on a polyester-toner microfluidic device. *Scientific reports* **2017**, *7*, 10466.
- [82] Liu, X. IR spectrum and characteristic absorption bands. *Organic Chemistry I; Kwantlen Polytechnic University: Surrey, BC, Canada* **2021**,
- [83] Rhimi, A.; Zlaoui, K.; Horchani-Naifer, K.; Ennigrou, D. J. Characterization and extraction of sodium alginate from Tunisian algae: synthesizing a cross-linked ultrafiltration membrane. *Iranian Polymer Journal* **2022**, *31*, 367–382.
- [84] Leal, D.; Matsuhiro, B.; Rossi, M.; Caruso, F. FT-IR spectra of alginic acid block fractions in three species of brown seaweeds. *Carbohydrate research* **2008**, *343*, 308–316.
- [85] Man, E.; Lamprou, D.; Easdon, C.; McLellan, I.; Yiu, H. H.; Hoskins, C. Exploration of dual ionic cross-linked alginate hydrogels via cations of varying valences towards wound healing. *Polymers* **2022**, *14*, 5192.
- [86] Wang, S.; Xing, Q. Study on properties and biocompatibility of poly (butylene succinate) and sodium alginate biodegradable composites for biomedical applications. *Materials Research Express* **2022**, *9*, 085403.
- [87] Irfanita, N.; Jaswir, I.; Mirghani, M. E. S.; Sukmasari, S.; Ardini, Y. D.; Lestari, W. Rapid detection of gelatin in dental materials using attenuated total reflection fourier transform infrared spectroscopy (ATR-FTIR). *Journal of Physics: Conference Series* **2017**, *884*, 012090.
- [88] Das, M. P.; Suguna, P.; Prasad, K.; Vijaylakshmi, J.; Renuka, M. Extraction and characterization of gelatin: a functional biopolymer. *Int. J. Pharm. Pharm. Sci* **2017**, *9*, 239.

- [89] Derkach, S. R.; Voron'ko, N. G.; Sokolan, N. I.; Kolotova, D. S.; Kuchina, Y. A. Interactions between gelatin and sodium alginate: UV and FTIR studies. *Journal of Dispersion Science and Technology* **2019**,
- [90] Jurić, S.; Đermić, E.; Topolovec-Pintarić, S.; Bedek, M.; Vinceković, M. Physicochemical properties and release characteristics of calcium alginate microspheres loaded with *Trichoderma viride* spores. *Journal of Integrative Agriculture* **2019**, *18*, 2534–2548.
- [91] Li, J.; He, J.; Huang, Y.; Li, D.; Chen, X. Improving surface and mechanical properties of alginate films by using ethanol as a co-solvent during external gelation. *Carbohydrate polymers* **2015**, *123*, 208–216.
- [92] Badita, C.; Aranghel, D.; Burducea, C.; Mereuta, P. Characterization of sodium alginate based films. *Rom. J. Phys* **2020**, *65*, 1–8.
- [93] Reay, S. L.; Jackson, E. L.; Ferreira, A. M.; Hilkens, C. M.; Novakovic, K. In vitro evaluation of the biodegradability of chitosan–genipin hydrogels. *Materials Advances* **2022**, *3*, 7946–7959.
- [94] Dimida, S.; Barca, A.; Cancelli, N.; Benedictis, V. M. D.; Raucci, M. G.; Demitri, C. Effects of Genipin Concentration on Cross-Linked Chitosan Scaffolds for Bone Tissue Engineering: Structural Characterization and Evidence of Biocompatibility Features. *International Journal of Polymer Science* **2017**, *2017*, 1–8.
- [95] Chen, Q.; Tian, X.; Fan, J.; Tong, H.; Ao, Q.; Wang, X. An interpenetrating alginate/gelatin network for three-dimensional (3D) cell cultures and organ bioprinting. *Molecules* **2020**, *25*, 756.
- [96] Peng, M.; Yang, M.; Ding, Y.; Yu, L.; Deng, Y.; Lai, W.; Hu, Y. Mechanism of endogenous digitalis-like factor-induced vascular endothelial cell damage in patients with severe preeclampsia. *International Journal of Molecular Medicine* **2018**, *41*, 985–994.
- [97] Condi Mainardi, J.; Rezwan, K.; Maas, M. Genipin-crosslinked chitosan/alginate/alumina nanocomposite gels for 3D bioprinting. *Bioprocess and Biosystems Engineering* **2022**, 1–15.
- [98] Ng, W.-C.; Lokanathan, Y.; Fauzi, M. B.; Baki, M. M.; Zainuddin, A. A.; Phang, S. J.; Azman, M. In vitro evaluation of genipin-crosslinked gelatin hydrogels for vocal fold injection. *Scientific reports* **2023**, *13*, 5128.